Acknowledgements

The following individuals at TRW contributed to the Two-Micron LAWS Pointing/Tracking Study:

Structural /Mechanical Modeling	Stenner Kleve Mike Waterman Walter Beckman
Dynamics Modeling	Ray Manning
Optical System	Martin Flannery
Controls Systems	Ron Mayo Reid Reynolds

I would like to express my appreciation to these individuals for their dedication and hard work which led to the successful completion of this study. I would also like to express my appreciation to Mr. Bill Grantham, the NASA/LaRC CoTR for his cooperation and guidance.

Scott Manlief
Program Manager

Table of Contents

TRW

Executive Summary

(This page intentionally blank)

do not film

Executive Summary

The Two-Micron Laser Atmospheric Wind Sounder (LAWS) Pointing/Tracking Study was performed by the Space & Technology Division , Space and Electronic Group of TRW for NASA LaRC under Contract No. NAS1-19291, MSOA Task No. 15. The period of performance of the study was from 1 January 1994 to 4 November 1994.

The objective of the study was to identify and model major sources of short-term pointing jitter for a free-flying, full performance 2μm LAWS system and evaluate the impact of the short-term jitter on wind-measurement performance. A fast steering mirror controls system was designed for the short-term jitter compensation. The performance analysis showed that the short-term jitter performance of the controls system over the 5.2 msec round-trip time for a realistic spacecraft environment was ≈ 0.3 μrad, rms, within the specified value of < 0.5 μrad, rms, derived in the 2μm LAWS System Study (6 October 1993).

Our approach was to develop a conceptual, yet detailed, structural and dynamics model for the 2μm LAWS instrument based on the results of the 2 μm LAWS System Study. As in the System Study, the basic optical form, including active beam jitter stabilization, proposed in the GE Phase II LAWS Study Final Report was assumed. The payload model was then merged with an existing spacecraft bus dynamics model for a TRW UAB-940 satellite and a modal analysis run out to 100 Hz. The full-performance 2 μm solid-state LAWS payload/AB-940 bus system is compatible with a Delta-class launch vehicle.

Disturbance models were defined for 1) the Bearing and Power Transfer Assembly (BAPTA) scan bearing, 2) the spacecraft reaction wheel torques , and 3) the solar array drive torques. The scan bearing disturbance was found to be the greatest contributing noise source to the jitter performance. Disturbances from the fast steering mirror reaction torques and a boom-mounted cross-link antenna clocking were also considered but were judged to be

(This page intentionally blank)

Executive Summary (con't)

small compared to the three principal disturbance sources above and were not included in the final controls analysis.

A fast steering mirror controls architecture was defined and loop parameters were defined to compensate for the line-of-sight pointing jitter induced by structural displacements excited by the three principal disturbance sources. The control loop design reduced the short-term X-axis open loop jitter over the 5.2 msec pulse round-trip time from an rms value of ≈2.4 μrad to ≈ 0.2 μrad when the loop was closed. The Y-axis jitter, both open and closed loop was found to be less than the short-term jitter about the X-axis. The Y-axis open-loop rms jitter was ≈ 0.5 μrad, and the residual short-term rms jitter when the FSM loop was closed was ≈ 0.2 μrad. The RSS value of the residual rms short-term jitter, then, is ≈ 0.3 μrad, meeting the specified jitter requirement of 0.5 μrad for the 2 μm LAWS system.

(This page intentionally blank)

2 μm LAWS Pointing/Tracking Study

2 μm LAWS Pointing/Tracking Study (NAS1-19291, MSOA Task No. 15); Period of Performance: 1 January 1994 to 4 November 1994

Objective

- Identify and model major sources of short-term pointing jitter for a free-flying 2 μm LAWS system and evaluate pointing-jitter impact on wind-measurement performance

Study approach

- Develop conceptual structural design and dynamics model for 2 μm LAWS instrument based on
  - 2 μm LAWS System Study results
  - Assuming basic optical form, including active beam jitter stabilization, proposed in GE Phase II LAWS Study final report

- Utilize existing dynamics model for a TRW UAB-940 spacecraft appropriately modified to accommodate the LAWS instrument

- Develop pointing controls model to evaluate jitter effects on system wind measurement performance incorporating as principal disturbance sources
  - Scan drive bearing noise
  - Fast steering mirror reaction torques
  - Spacecraft reaction wheels unbalance and torques
  - Solar array stepping
  - Boom-mounted cross-link antenna

(This page intentionally blank)

Requirements Summary

(This page intentionally blank)

(This page intentionally blank)

LAWS Pointing Requirements

The LAWS pointing accuracy and pointing knowledge requirements are set by geometrical considerations and are independent of the operating wavelength of the lidar.

The LAWS pointing accuracy requirement is set by the mission shot density requirement of 3 pulse pairs per 100 km grid or, effectively, a target area approximately 30 km square. For the 525 km orbit and a scan angle of 45°, the pointing accuracy requirement is approximately ± 14 μrad.

The pointing knowledge requirement is determined by the requirement that fluctuations in the component of the spacecraft velocity vector along the pointing line of sight (LOS) be small compared to the desired LOS wind velocity measurement accuracy. Spacecraft LOS velocity errors may be introduced, for example, by fluctuations in the ephemeris or in the spacecraft attitude.

The limiting pointing knowledge requirement occurs when the line of sight is perpendicular to the orbital plane. To limit the contribution from spacecraft velocity fluctuations to less than 0.25 m/s, the pointing knowledge must be known to less than ±36 μrad.

LAWS Pointing Requirements

Pointing accuracy and knowledge requirements are independent of the lidar wavelength

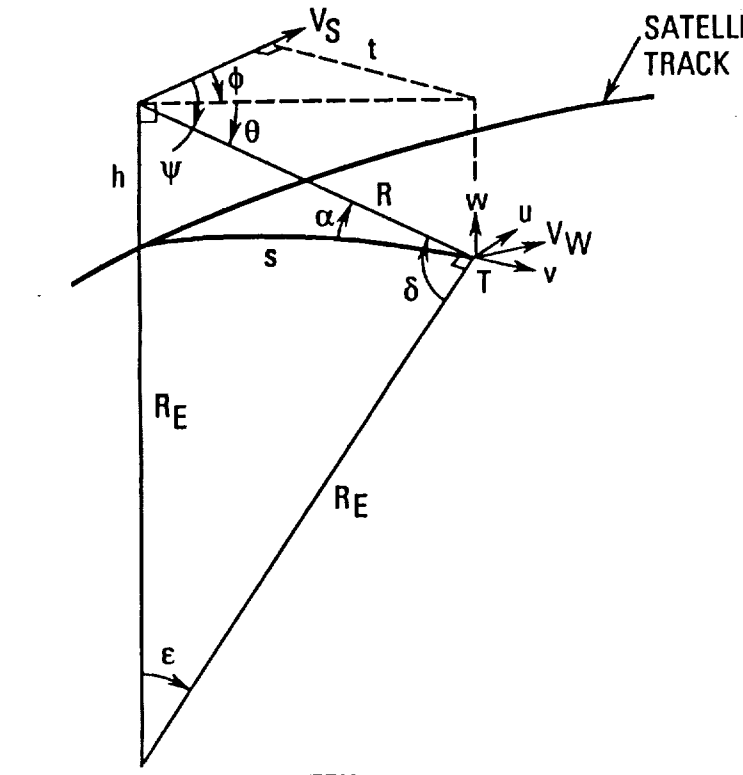

CONICAL SCAN GEOMETRY

- Pointing angle, ψ, accuracy requirement to target 30 km area = $\pm$ 14 mrad
- Pointing knowledge requirement determined by requirement that the LOS component of spacecraft velocity errors introduced by ephemeris or attitude fluctuations be small compared to the desired LOS wind velocity measurement accuracy of $\pm$ 1 m/s

$$(\Delta V_{LOS}) = \Delta(V_S \cos\Psi) = V_S \sin\Psi \Delta\Psi$$

- Limiting knowledge requirement when pointing perpendicular to spacecraft velocity vector
- For $\Delta V_{LOS} < \pm$ 0.25 m/s

$$\Delta\Psi \leq \frac{0.25}{V_S \sin\Psi} = \pm 36 \mu rad$$

Short-Term Jitter Requirement Scales as Wavelength

In contrast to the pointing accuracy and knowledge, the short-term jitter requirement scales directly with the operating wavelength of the lidar. Physically, the receiver must maintain stable pointing toward the aerosol scattering volume during the pulse round-trip time to minimize differences between the received backscatter signal and the local oscillator phase fronts. The effect of phase-front misalignments is to reduce the heterodyne mixing efficiency and consequently the received signal-to-noise.

Imposing the requirement that the short-term jitter must be less than ≈ 1/10th of the transmit beam divergence (= 2.44 λ/D) results in jitter requirement values of 0.5 μrad and 1.5 μrad for aperture values of 1.33 m and 1.5 m at wavelengths of 2.06 μm and 9.1 μm, respectively.

Our WindSounder performance model calculates the effect of jitter misalignment on heterodyne mixing efficiency. The results of the jitter analysis are shown below. For rms jitter values of 0.5 μrad and 1.5 μrad, the mixing efficiency is reduced by ≈ 0.3 dB and ≈ 0.2 dB at 2.06 μm and 9.1 μm, respectively.

Short-Term Jitter Requirement Scales as Wavelength

Requirement is that receiver maintain stable pointing toward scattering volume (defined by transmit spot diameter) during round-trip time of 5.2 msec

- Jitter effect is to reduce heterodyne mixing efficiency and consequently received SNR

Short-term jitter requirements of 0.5 μrad and 1.5 μrad for 2.06 μm and 9.1 μm, respectively, defined in 2 μm LAWS System Study (Oct 93) and the GE Phase II Study Final Report (Sept 92)

- Corresponds to approximately 1/10th of the transmit beam divergence ($\propto \lambda/D$)

WindSounder performance model analysis shows rms jitter values of 0.5 μrad and 1.5 μrad reduce mixing efficiency by ~ 0.3 dB and ~ 0.2 dB for 2.06 μm and 9.1 μm, respectively

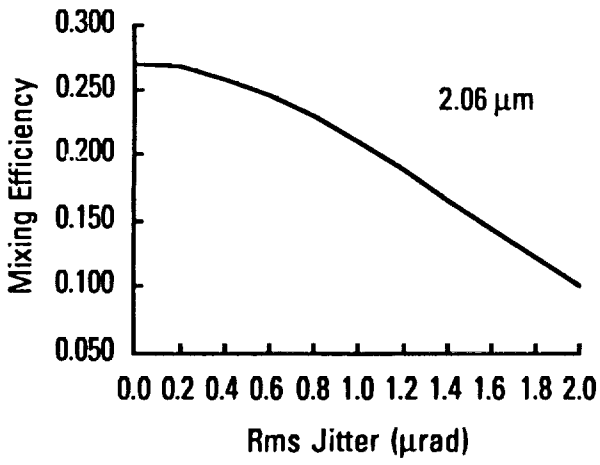

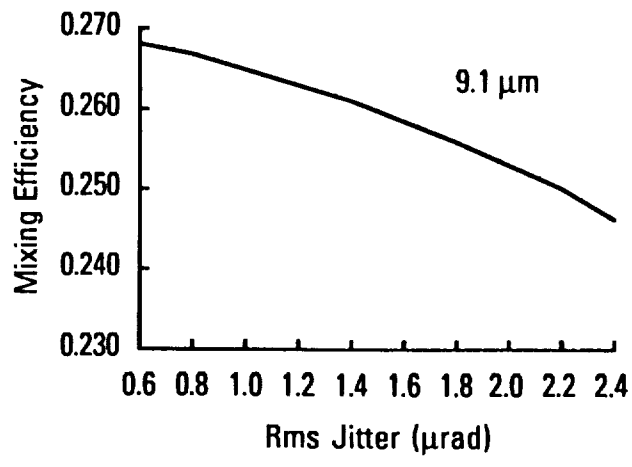

Fast Steering Mirror (FSM) Requirements

The short-term pointing jitter applies to the closed loop residual error over the return pulse round-trip time of 5.2 msec. There is also the requirement that the receive pulse be on the receiver detector. Thus the IMC tracking loop must meet the jitter requirement over 5.2 milliseconds. A typical spacecraft induced boresight motion at low frequency is 200 μrad. For a optical magnification of 33 this corresponds to a mirror travel of 3300 μrad which is interpreted as the amplitude of the sinusoidal mirror motion. The receiver open loop jitter is defined for an inertial laser source and is governed by the tracking mirror travel limit and the acceleration capability of the FSM torque mechanism. Other considerations are the pulse echo duration (≈ 200 μsec) and the loop bandwidth. The allocated short-term jitter for the FSM is 0.28 μrad (1σ). As an example, suppose the receiver open loop jitter at 10 Hz relative to an inertial source is 8.2 μrad (1σ). Then the estimated steady state closed loop performance is

$$\text{Estimated closed loop performance} = (8.2/82) \times 0.28 = 0.028\ \mu\text{rad}$$

The noise floor on the curve shown is set by the reaction torque noise which, under operational conditions, is ≤ 10 nrad (far-field) across the frequency range shown (assuming pulse-width-modulated drives operating above 20 kHz)

Fast Steering Mirror (FSM) Requirements

Typical spacecraft vibration levels suggest that the FSM (image motion compensator) disturbance rejection capability at low frequencies be set at ≈ 200 μrad

Asymptotic plot of allowed target space LOS jitter vs. frequency, using a 0.28 μrad (1σ) jitter allocation over 5.2 msec (pulse round-trip time), a travel limit of 3300 μrad, a mirror acceleration limit of 500 rad/sec^2, and a tracking loop bandwidth of 500 Hz given by

LAWS IMC LOOP SINE SWEEP CAPABILITY

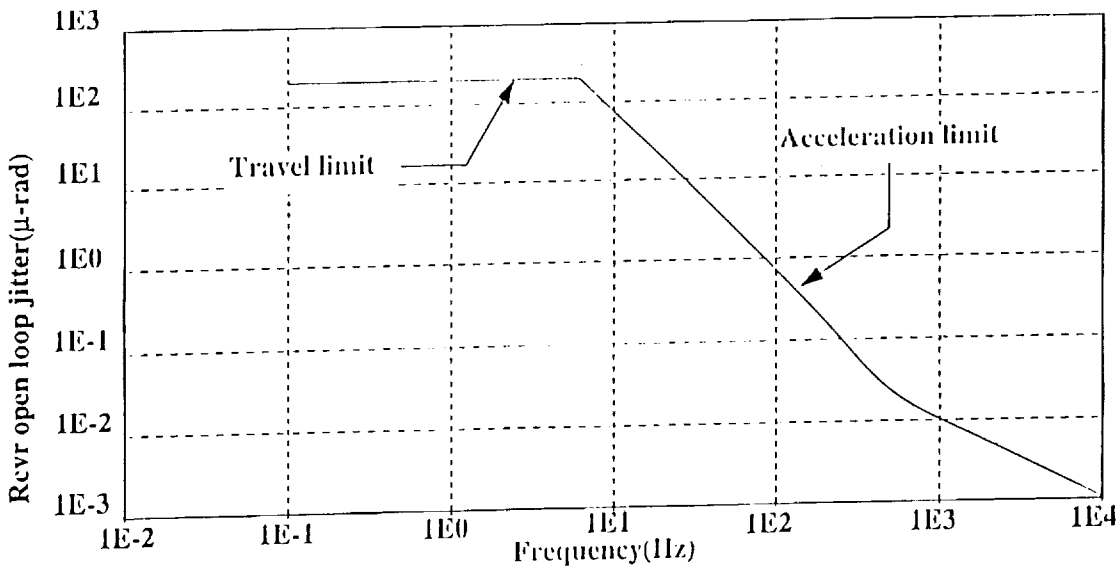

FSM Requirements - II

The IMC loop LOS sine sweep capability plot shown on the previous vugraph is for a single disturbance frequency. If there are multiple frequencies, the allowable amplitudes must be reduced in accordance with the sum expression shown.

The required range of travel is 3300 μrad in local space for a low frequency target space variation of 200 μrad; the required travel with 20% margin becomes 3960 μrad.

The steering mirror size depends on the aperture diameter and the telescope magnification. The mirror is elliptical since it is tilted at 45° to the incident beam.

FSM Requirements - II

- If there are multiple frequencies f_i, 1 = 1,...,n, with amplitudes a_i, respectively, the normalized sum shall be less than one

$$\sum_{i=1}^{n}\left(\frac{|a_i|}{r(f_i)}\right)\leq 1$$

  where $r(f_i)$ is the requirement from the single sine sweep curve at frequency f_i

- Range of travel shall be at least ± 3960 μrad (local) with 20% margin

- The steering mirror size dictated by

  - 1.33 meter aperture
  - 33x magnification
  - 20% margin

  shall be at least 1.9 x 2.7 inches elliptical

(This page intentionally blank)

Structural/Mechanical/Dynamics Modeling

(This page intentionally blank)

(This page intentionally blank)

2 μm LAWS Instrument Assembly

A conceptual structural model of the 2 μm LAWS instrument assembly, which conforms to the design parameters derived in the 2μm LAWS System Study, was developed to serve as the basis for a simplified dynamics model. The instrument model was integrated with a modification of existing spacecraft structural dynamics model for TRW's UAB-940 bus.

The structural model for the LAWS instrument was developed using our ARIES computer-aided design tool. Individual elements were modeled as solids with appropriate densities assigned. The use of the ARIES tool provided automated calculation of mass properties and center-of-gravity (c.g.) locations for individual elements and/or assemblies.

As shown in the figure, the major sub-assemblies of the instrument mechanical system are:

- The primary and secondary mirrors with the metering structure
- The telescope support structure
- The bearing and power transfer assembly (BAPTA) with derotator and transfer optics bench
- The laser transmitter and receiver assembly
- The instrument support structure

2 μm LAWS Instrument Assembly

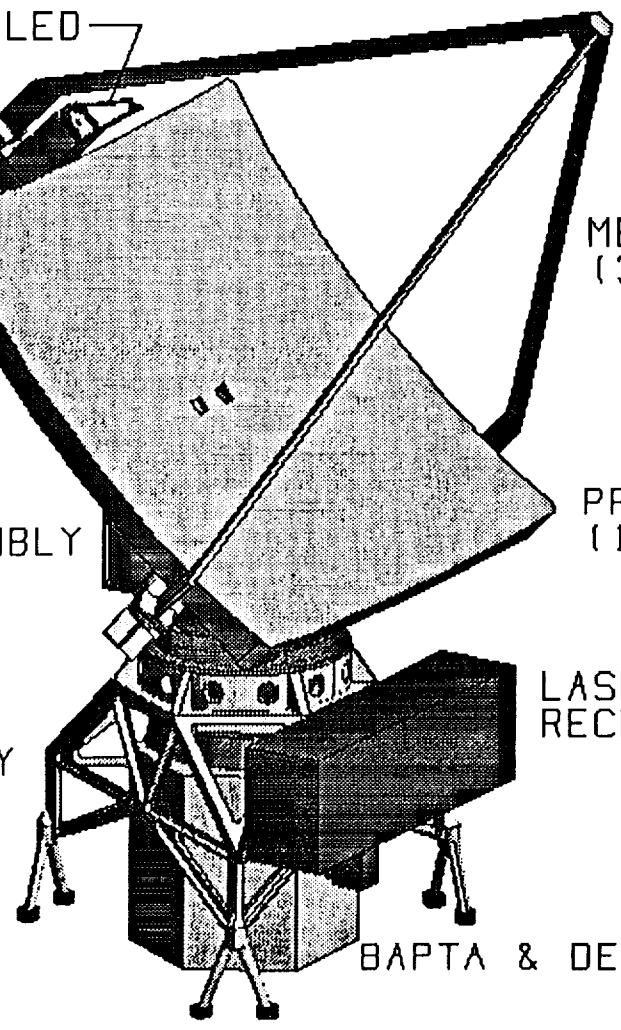

2 μm LAWS Instrument - Exploded Assembly

This exploded view is a better illustration of the various elements of the instrument mechanical subsystem, showing the full extent of the telescope support assembly.

The rotor in the BAPTA, which is a large diameter hollow shaft, supports the scanning elements--the telescope support assembly, the primary and secondary mirrors and the metering structure. The stationary part of the BAPTA supports the derotator assembly and the optical bench including the image motion compensator fast steering mirror (FSM), the lag angle fast steering mirror (LAFSM) and the shot vector sensor.

The complete BAPTA with the scanning elements are coupled to the laser transmitter and receiver assembly via the instrument support structure. The interface from the structure to the BAPTA is a flanged ring, and the interface from the structure to the laser assembly is a 3-point attachment directly from the structure to the optical bench in the laser assembly.

For the primary mirror, which is a complex, highly light weighted Be structure, the total weight was estimated by scaling the results in the GE Phase I final report. A derived density was assigned to our mirror model to yield the estimated weight. This permitted a reasonably accurate calculation of the inertia values.

For the BAPTA, derotator and the optical bench with associated components, weights and mass distributions were estimated from data in the GE Phase I final report.

2 μm LAWS Instrument - Exploded Assembly

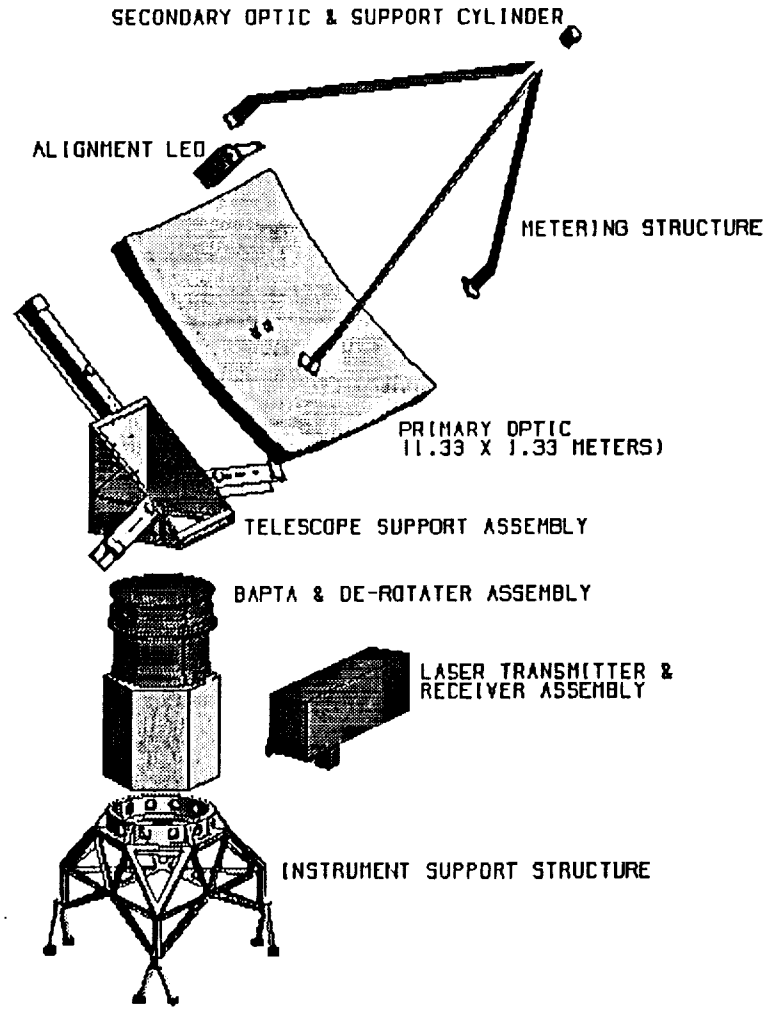

Laser Transmitter and Receiver Assembly

The conceptual structural design for the laser transmitter and receiver assembly was based on an 8.2 J/pulse, two-pulse burst system defined in the 2 μm LAWS System Study as required to provide a LOS wind velocity measurement accuracy of ± 1 m/sec. As shown, the laser transmitter and receiver subsystems are mounted on opposite faces of a single optical bench. Weights and sizes of individual components and subassemblies were anchored to either manufacturers specifications or existing hardware for breadboard laser systems.

The total weight of the assembly is estimated to be 87 kg. The weight model was based on detailed point designs developed by TRW for space-based and military laser systems. The internal subassemblies, the optical bench and the housing were modeled as solid prisms and cylinders using estimated densities based on the type of subassembly.

Laser Transmitter and Receiver Assembly

Conceptual structural design based on

- 8.2 J/pulse, two-pulse burst system as defined in 2μm LAWS System Study
- Results of TRW design studies for space-based laser systems
- Manufacturers specifications or existing hardware for breadboard laser systems

Laser transmitter and receiver subsystems mounted on opposite faces of single optical bench

- Total weight of assembly: 87 kg
- External dimensions of assembly: 35.6 x 11.3 x 8.3 inches

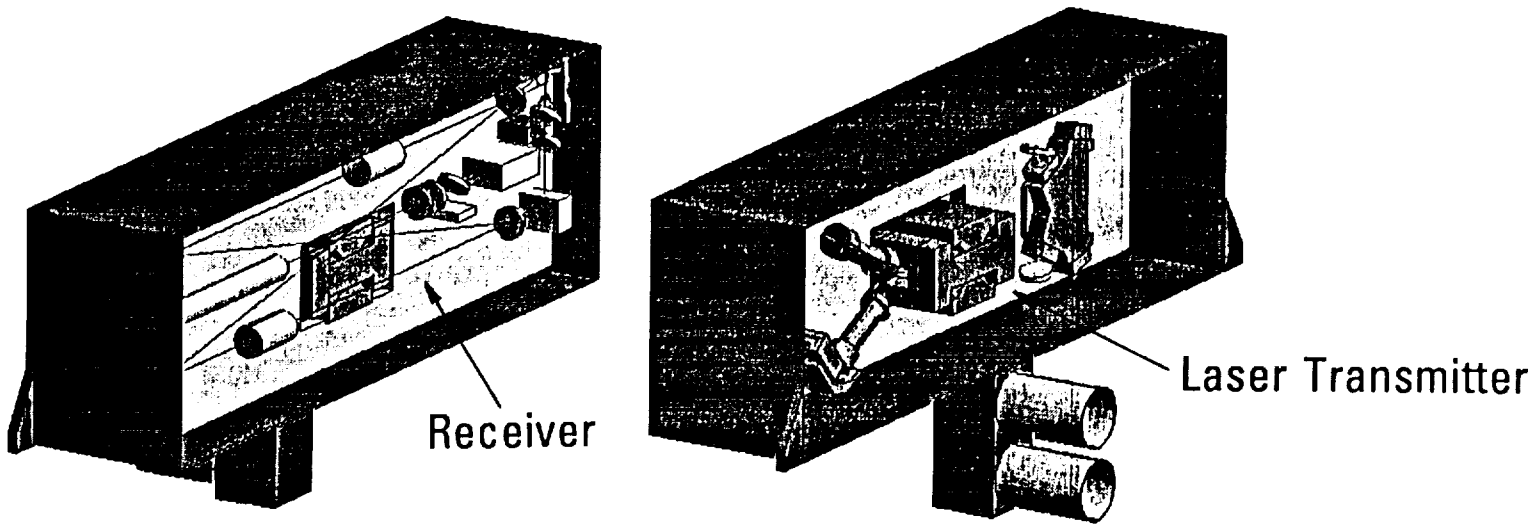

2 μm LAWS Launch Configuration

The LAWS instrument is shown in the launch configuration on the TRW UAB-940 spacecraft bus placed on a Delta launch vehicle with a 110 inch I.D. fairing.

A kinematic mechanical interface with the spacecraft was designed which consists of three bipod struts extending from the instrument support structure. The launch loads are transmitted from the bipods via shear webs into the 940 mm central tube in the spacecraft.

This design greatly reduces loads on the instrument due to thermal distortions of the spacecraft. It does not, however, eliminate instrument pointing errors due to such distortions. In a detailed design, careful consideration would be given to the optimal placement of navigation equipment such as star trackers and inertial measurement units. The design also facilitates thermal isolation of the instrument from the spacecraft should this be desirable.

2 μm LAWS Launch Configuration

2 μm LAWS instrument mounted on a TRW UAB-940 bus can be accommodated mechanically on a Delta launch vehicle

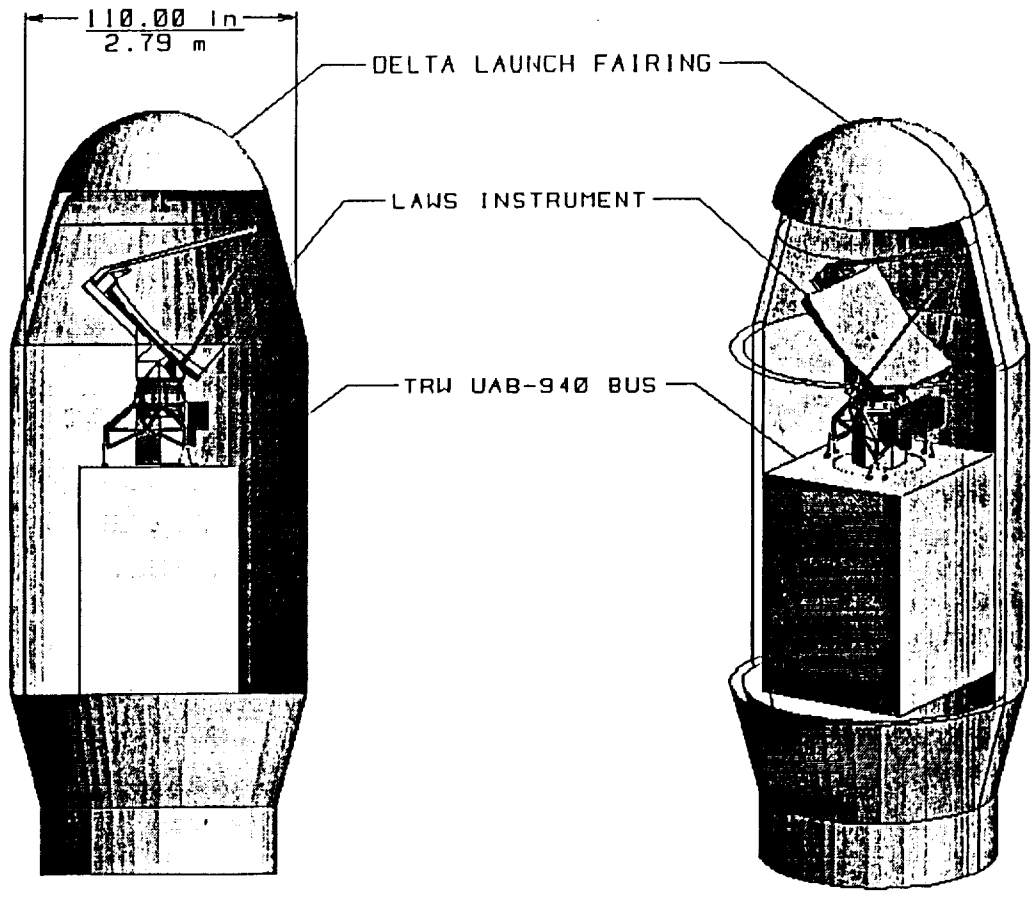

2 μm LAWS Instrument Mass Properties

The output from the mechanical design task was provided for the payload dynamics model which was merged with the LAWS system dynamics model. These data consisted of the geometry for the instrument and for individual elements where required. Also provided were the mass, the center-of-gravity (CG) location and the mass moment of inertia about three axes for individual elements as shown in the vugraph.

The size and material properties of structural members were also provided. These members were resized to improve the structural model after preliminary runs of the dynamics model.

LAWS Instrument Mass Properties

Component	Mass		CG*			I_x	I_y	I_z
	Lb_m	kg	x (in)	y (in)	z (in)	Lb_m-in^2		
Primary Mirror	150	68	-2.93	54.81	0	5.1E5	6.4E4	4.9E5
Secondary Mirror Assy	15.4	7	39.04	96.78	0	1.4E5	2.3E4	1.7E5
Telescope Support	87.4	40	-3.72	45.33	0	2.0E5	1.7E4	2.0E5
Metering Structure	21.4	10	14.4	72.17	0	1.2E5	1.7E4	1.3E5
LED Alignment Assy	4.5	2	-21.76	76.16	0	2.6E4	2.2E3	2.8E4
Telesccpe Assembly	279	127	0	55.85	0	1.0E6	1.2E5	1.0E6
BAPTA	496	225	0	17.95	0	4.8E5	4.7E4	4.8E5
Structure Assy	79.2	36	0	21.02	0	4.0E4	1.4E4	4.0E4
Laser/Receiver Assy	191	87	15.98	20.75	-.03	7.8E4	5.2E4	9.8E4
Instrument Assembly	1045	475	2.31	29.34	0	1.6E6	2.4E5	1.6E6
Digital Electronics	11	5	NA			NA		
ADS	37	17	NA			NA		
Electrical	64	29	NA			NA		
Thermal	196	89	NA			NA		
Contingency	55	25	NA			NA		
Total System	1408	640	NA			NA		

* Origin is on spin axis at level of spacecraft interface

2 μm LAWS System Finite Element Model
Model Overview

The principal elements of the 2 μm Laser Atmospheric Wind Sounder (LAWS) mission model consists of the LAWS payload including the Bearing and Power Transfer Assembly (BAPTA), two Fokker 1 kW solar arrays, a space to ground link (SGL) antenna and the spacecraft bus.

The on-orbit configuration of the 2 μm LAWS system finite element model is shown on the vugraph. The LAWS payload is mounted on the nadir panel (+Z panel) of the spacecraft bus with the boresight axis oriented 45° above the Y axis in the YZ plane. A modification of a structural dynamics model for the TRW UAB-940 spacecraft bus was used in the study. The UAB-940 spacecraft model was stripped of its appendages and converted to a nadir-pointing system. The original solar arrays were replaced with the Fokker solar arrays (discussed later) because the original arrays were unsuited to the LAWS mission requirements. The TDRS-Flight 7 SGL replaced the original 940 ground links because they were designed for a zenith-pointing system.

The payload itself is comprised of primary and secondary mirrors, a laser/receiver assembly, an LED boresight alignment source, the BAPTA and a support structure. The support structure is used to align and hold the transfer optics of the payload as well as to mount the payload (through the BAPTA) to the spacecraft bus. Scan motions of the payload relative to the spacecraft are allowed through the BAPTA. Derotator rotations relative to the optical bench about the Z axis are also allowed.

Two 1 kW Fokker solar array wings are mounted onto the spacecraft bus and oriented along the +Y and -Y axes with their outward normals parallel to the Z axis. A SGL reflector system for space to ground communication is also mounted onto the spacecraft bus with the SGL boom along the +X axis.

2 μm LAWS System Finite Element Model

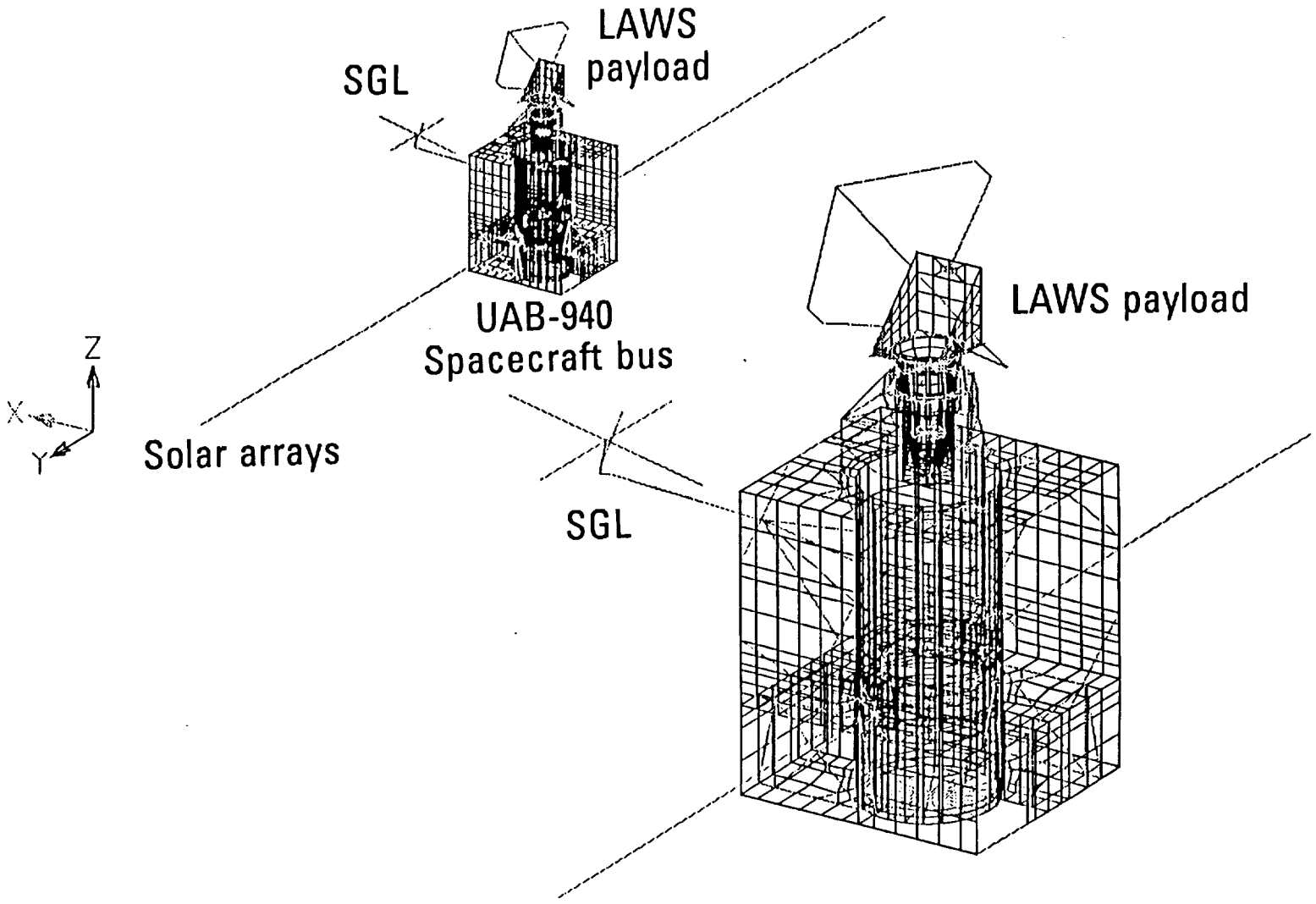

LAWS Payload Finite Element Model

A finite element model of the LAWS instrument assembly was constructed from the conceptual structural design described previously. The primary mirror and secondary mirror were each modeled as concentrated masses and rotational inertias. Whereas the secondary mirror is integral with the metering truss, the primary mirror is mounted through stiff bars (representing a rigid mirror) and elastic springs. The elastic spring elements were tuned to yield first primary tip and tilt modes near 70 Hz.

Initial sizes for all structural members were scaled from available conceptual level drawings. These sizes were then updated to yield the expected modal content of the instrument system.

LAWS Payload Finite Element Model

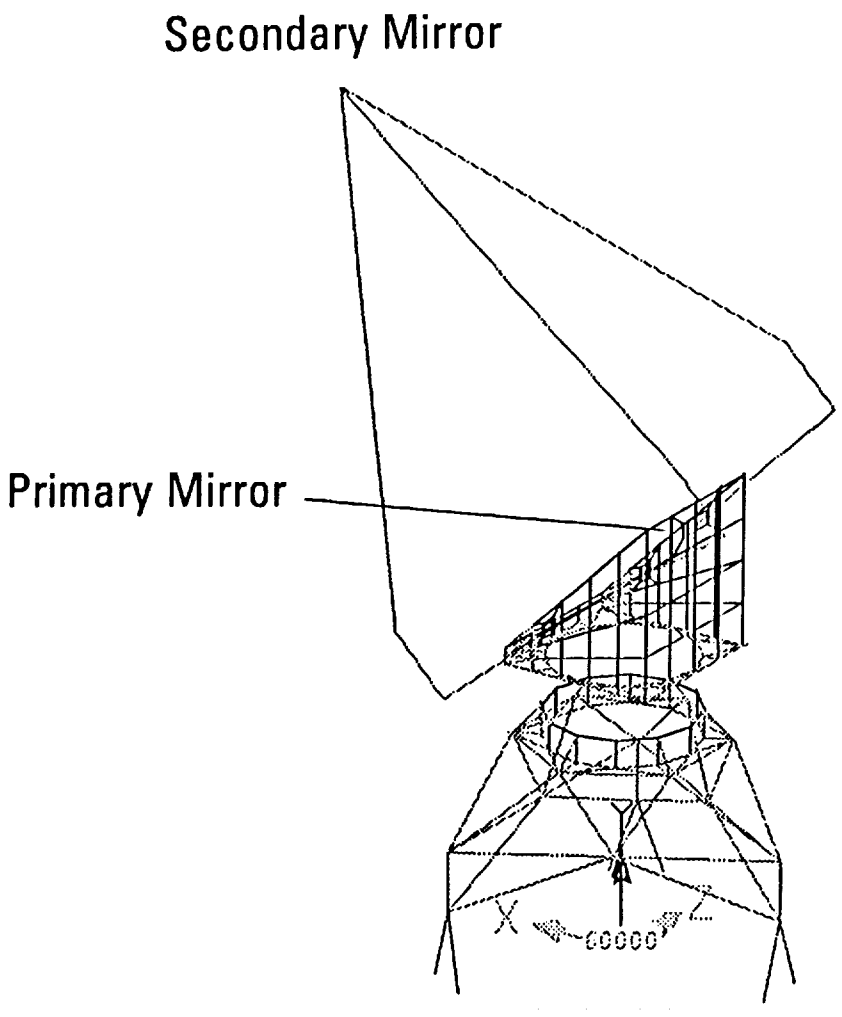

Bearing and Power Transfer Assembly (BAPTA) Model

A finite element model of the BAPTA was created and run using a NASTRAN static analysis The model is composed of 259 nodes and 228 shell elements. The shell elements are used to represent the structural parts of the BAPTA--the housings, the shafts and the optical bench. Cylindrical or conical elements are divided into 12 elements around their circumference (i.e., each flat shell element represents an arc of 30°).

The bearings (discussed on following vugraphs) are represented by spring elements that join the OD to the ID of the bearing. Radial, axial and moment stiffnesses are modeled.

Non-structural masses (i.e., the mass of items not modeled as shell elements in the structural load path) such as the bearings, resolvers, motors, and mirrors, are roughly represented in the model by an increase in the density of neighboring shell elements. These non-structural masses account for a significant fraction of the total estimated weight of the BAPTA. For the NASTRAN model which was used to obtain the compliance matrix for the BAPTA, the housings and shafts were assumed to be titanium, the optical bench was assumed to be aluminum and the bearing were assumed to be steel. The estimated weight of the BAPTA is 496 lb. The CG is estimated to be on the symmetry axis, 17.5 inches from the payload interface.

The BAPTA contains two rigid body modes; 1) one for the scan rotation of the LAWS instrument relative to the spacecraft, and 2) one for the scan rotation of the derotator relative to the optical bench. In the dynamics analysis, the turning and fold mirrors were considered rigidly attached to the optical bench portion of the BAPTA. Derotator periscope flats and turning mirrors were considered rigidly attached to the derotator. Bearing stiffnesses between the BAPTA housing and payload shaft and between the optical bench and derotator were estimated from BAPTA drawings and previous experience. With the BAPTA model unconstrained, eight rigid body modes are obtained with the first flexible mode near 200 Hz.

Bearing and Power Transfer Assembly (BAPTA) Model

BAPTA model including derotator and transfer optics bench constructed based on
- Drawings included in the GE Phase I and Phase II final reports
- TRW experience with similar units

BAPTA NASTRAN FEM model description
- 259 node, 228 shell elements
- Bearings represented using CELAS2 elements and MPCs
- Housings and shafts are assumed to the titanium
- Optical bench assumed to be aluminum
- Non-structural masses (bearings, resolvers, motors, etc.) simulated by increasing density of neighboring shell elements

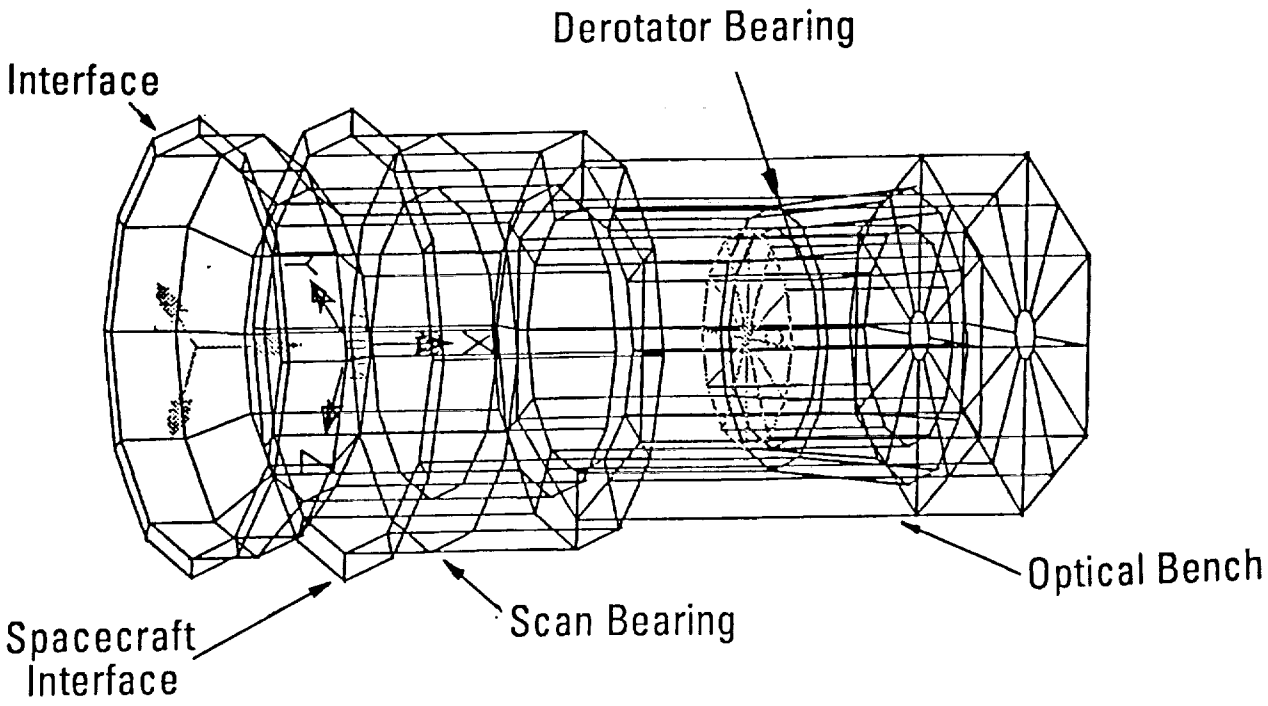

Estimated Characteristics Of BAPTA Bearings

The dimensions of the scan and derotator bearings were scaled from a drawing of the BAPTA in the GE Phase II final report.

SCAN BEARING

The number of balls per bearing was estimated based on experience with other duplex bearings. The weight was estimated by calculating the volume of material in the bearing and balls and multiplying by the density of steel. A weight of 40 lb for the pair was calculated. This appears to be a custom bearing--no catalog item was found that matched this bearing.

The stiffness of the bearing is influenced by a variety of factors that cannot be scaled from the drawing, such as pre-load, race curvature and contact angle. To estimate the stiffnesses, race curvatures of 0.53 and 0.52 were used for the inner and outer races, respectively. A contact angle of 20° was assumed. Preloads of 60 lb and 600 lb were evaluated, and stiffnesses were assigned based on an intermediate value.

DEROTATOR BEARING

A catalog bearing matching the scaled dimensions of the derotator bearing was located. The estimated weight of 13 lb for the pair was determined as above.

Assumptions concerning race curvature, contact angle and preload for the bearing are: outer and inner race curvature are 0.535 and 0.525, respectively. The contact angle is 20° and the preload is assumed to be 60 lb.

Estimated Characteristics of BAPTA Bearings

Scan Bearing	Derotator Bearing
Estimated dimensions/characteristics OD: 16.0 in ID: 13.1 in Pitch diameter: 14.6 in Ball row separation: 10.275 in Ball diameter: 0.875 in Number of balls: 40 Weight: 40 lb (for the pair)	Estimated dimensions/characteristics OD: 10.5 in ID: 9.0 in Pitch diameter: 9.75 in Ball row separation: 0.75 in Ball diameter: 0.375 in Number of balls: 62 Weight: 13 lb (for the pair)
Stiffnesses Axial: 1.0×10^6 lb/in Radial: 3.6×10^6 lb/in Moment: 190×10^6 lb-in/rad	Stiffnesses Axial: 0.67×10^6 lb/in Radial: 2.36×10^6 lb/in Moment: 11.4×10^6 lb-in/rad

BAPTA Compliance Matrix

In order to determine the compliance of the BAPTA, a unit load centered on the axis was applied to the payload interface and reacted at the spacecraft interface. Displacements and/or rotations were measured at the point of load application (on the axis at the payload interface). Items included in the load path are the scan bearing, the housing from the center of the scan bearing to the spacecraft interface and the shaft from the center of the scan bearing to the payload interface. The bearing was considered free to rotate, so terms in the compliance matrix related to rotation of the bearing were set equal to zero. Almost all off-diagonal terms were effectively zero. The one exception is that some coupling between radial loads and bending exists, as would be expected.

Since the model is based on scaled dimensions and several assumptions (materials for housing and shafts, bearing preloads, number of balls, etc.) the calculated compliance values could vary as much as ±50% from the actual BAPTA.

BAPTA Compliance Matrix

Estimated compliances between the spacecraft interface and payload interface

- x = axial direction
- Terms less than 10^{-12} set to zero
- Bearings are assumed to be free to rotate

	d_x (in)	d_y (in)	d_z (in)	Rot_x (rad)	Rot_y (rad)	Rot_z (rad)
F_x: 1.0 lb	1.27 E-6	0	0	0	0	0
F_y: 1.0 lb	0	1.34 E-6	0	0	0	-1.03 E-7
F_z: 1.0 lb	0	0	1.34 E-6	0	1.03 E-7	0
M_x: 1.0 in-lb	0	0	0	0	0	0
M_y: 1.0 in-lb	0	0	1.03 E-7	0	1.48 E-8	0
M_z: 1.0 in-lb	0	-1.03 E-7	0	0	0	1.48 E-8

Appendages

Two flexible appendages were used in developing the LAWS on-orbit system model. The first was a simplified model of a set of Fokker solar arrays and the second was a model of a ground link antenna.

Two 1 kW Fokker solar array wings were determined to be adequate to meet the power requirements of the 2 μm LAWS mission. Each wing weighs 54 lbs and has two panels measuring 126 x 63 inches. The inboard panel is mounted to the spacecraft bus through a 110 inch long yoke and Solar Array Drive Assembly (SADA). The rotational stiffness of the SADA was set at 100000 in-lbs/rad in the torsional (i.e., clocking) axis and 250000 in-lbs/rad in the two orthogonal bending axes. A detailed model of the Fokker array was taken from an existing spacecraft program and used to derive a simplified "stick" model. The stick model has inertial properties equivalent to the detailed model and was tuned to yield approximately equivalent modes. Thus tuned, the first out-of-plane bending modes of the solar arrays when fixed at the inboard side of the SADA were 0.33 Hz, with the first in-plane bending modes at 0.59 Hz and first torsional modes at 2.08 Hz.

A simplified model of a space to ground link (SGL) reflector/boom subsystem was taken from TRW's TDRS-Flight 7 model and modified for use in the LAWS analysis. The weight of the SGL system, which consists of a 4 foot reflector, a feed, a boom and a biaxis drive unit, was scaled down from the TDRS value of 40 lbs to 25 lbs. This scaling was done to reflect design and material changes for the latest TDRS constellation of satellites. The SGL was mounted to the spacecraft bus in a manner such that it can be stowed without interfering with the bus or payload and can deploy into the proper orientation to establish the ground link. Rotational stiffness values of the biaxis drive unit were taken directly from the TDRS-Flight 7 model and were 5464000 in-lbs/rad, 3850000 in-lbs/rad, and 2500000 in-lbs/rad about the scan, elevation and bending axes (X, Y, and Z axes), respectively.

Appendages

Two flexible appendages incorporated into the LAWS on-orbit system model

- A pair of solar array wings (two 1 kW arrays)
- A space to ground link (SGL) communication antenna

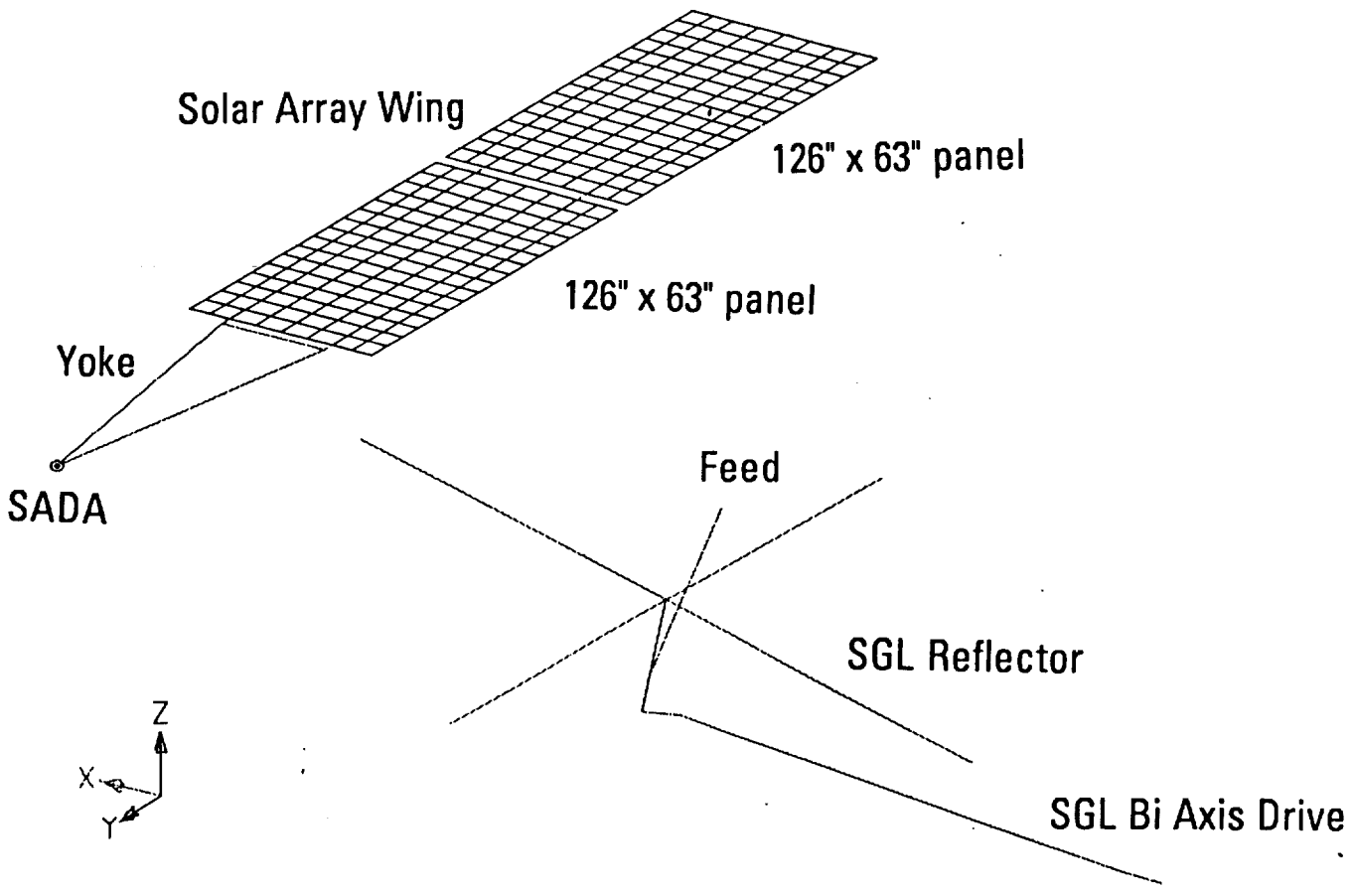

Key LAWS Finite Element Model Points

The LAWS finite element model was reduced to modal space using all 112 modes below 100 Hz. Only key points with the LAWS system was used for the open and closed loop jitter simulation to reduce the size and runtime of the simulation.

The points that were retained in the jitter model include all the optical elements, the points where disturbances are to be injected and other points of interest. The vugraph summarizes the key points that were retained and their locations on the spacecraft.

Key LAWS Finite Element Model Points

Grid Number	Description	Location (in)		
		X	Y	Z
1001	Separation plane	0.0	0.0	0.0
1005	Fuel tank CG	0.0	0.0	62.9
2283	RWA assembly	-16.1	-9.32	28.2
17021	Inboard +Y SADA point	0.0	23.2	34.8
19021	Inboard -Y SADA point	0.0	-23.2	34.8
31001	Outboard +Y SADA point	0.0	23.2	34.8
32001	Outboard -Y SADA point	0.0	-23.2	34.8
46013	Outboard SGL BiAx drive point	-51.8	0.0	63.3
56007	Inboard SGL BiAx drive point	-51.8	0.0	63.3
60000	Secondary mirror	0.0	40.8	185.0
61000	Primary mirror	0.0	-2.9	141.4
60042	LED assembly	0.0	-24.5	156.9
60399	Telescope side of BAPTA	0.0	0.0	123.3
65199	Spacecraft side of BAPTA	0.0	0.0	116.7
70097	Telescope side of BAPTA	0.0	0.0	123.3
70100	Spacecraft side of BAPTA	0.0	0.0	116.7
70201	Derotator	0.0	0.0	98.2
70260	Optical bench of BAPTA	0.0	0.0	87.3

Jitter and Stability Analysis

The 2 μm LAWS payload, BAPTA, appendages and the modified UAB-940 bus models were integrated to form the LAWS system used for the on-orbit jitter and stability analysis. The resulting LAWS system model has the inertial properties shown in the table.

2 μm LAWS System Inertia Properties			
Weight (lbs)	5618		
CG Location* (in)	X = 0.53	Y = 0.43	Z = 56.7
Inertia Matrix** (lbs-in^2)	1.62E7	-1.78E4	-5.43E4
	-1.78E4	8.95E6	-1.63E5
	-5.43E4	-1.63E5	9.19E6

* Relative to spacecraft separation plane
** Relative to spacecraft CG

The complete system model was found to be free from grounding when run in the free-free (i.e., on-orbit) condition. Eigenvalue extraction runs yielded eight rigid body modes for the complete system, one for the payload scan relative to the spacecraft, and one for the derotator scan relative to the optical bench. The first flexible modes of the system started at 0.33 Hz and were predominantly solar array out-of-plane, in-plane and torsional modes. Running the eigenvalue extraction out to 100 Hz yielded 112 total modes (i.e., eight rigid body modes and 104 flexible modes.

Jitter and Stability Analysis
Selected Mode Descriptions

Mode Number	Frequency (Hz)	Description
1-6	0.0	System rigid body modes
8	0.00	BAPTA rigid body modes
9	0.33	Solar array out-of-plane bending (Sym)
10	0.42	Solar array out-of-plane bending (Asym)
11	0.59	Solar array in-plane bending (Sym)
12	1.20	Solar array in-plane bending (Asym)
13	1.83	Solar array out-of-plane bending (Sym)
14	1.85	Solar array out-of-plane bending (Asym)
15	2.09	Solar array torsion (Sym)
16	2.41	Solar array torsion (Asym)
17	5.31	Solar array out-of-plane bending
18	5.32	Solar array out-of-plane bending
19	6.87	Solar array torsion
20	6.87	Solar array torsion
21	8.65	Solar array in-plane bending
22	8.75	Solar array in-plane bending
23	8.89	Solar array torsion
24	8.89	Solar array torsion
25	11.2	Solar array out-of-plane bending
26	11.2	Solar array out-of-plane bending
27	11.9	SGL Y bending
28	12.9	SGL Z bending
29	13.6	Payload Y bending
30	14.7	Payload X bending, SGL mode
31	15.7	SGL torsion
32	16.6	Metering truss mode

Strain Energy Analysis and Passive Damping Treatment

In running dynamics and control loop simulations, a number of modes were found to present difficulties in closing the fast steering mirror control loops or in blending sensor measurements. The strain energy distribution for these various modes was investigated so that minor redesign, such as increasing localized stiffness or local passive damping treatment could be applied.

For the sensor blending task, a mode near 0.4 Hz caused phase loss problems. Examination of modes in this frequency region indicates that both symmetric and asymmetric solar array out-of-plane bending modes occur near 0.4 Hz. The mode shapes themselves indicate that the symmetric mode is benign as it causes no significant motions of the spacecraft bus or LAWS payload. On the other hand, the asymmetric mode causes a rocking of the spacecraft bus/LAWS payload about the X axis. This rocking motion is the cause of the phase loss. Ten percent of the strain energy of the asymmetric bending mode is contained within the SADA. Therefore, the addition of a passive, viscoelastically damped joint damper at the base of the solar arrays would be a good candidate to minimize the effects of this mode on the sensor blending task. Using a conservative loss factor of 0.7, one could expect to obtain 7% damping in this mode using a joint damper. Furthermore, with the addition of a joint damper at the base of the solar array, all solar array modes would have increased damping levels. The final damping levels obtained would be dependent on the amount of strain energy in the passive joint and the loss factor of the viscoelastic material used in the joint.

For the design of the fast steering mirror control loops, modes at 8.3 and 10.8 Hz were found to limit performance and stability. These modes were examined and found to be primarily payload bending modes. In each mode the LED source and the secondary mirror were moving a significant amount, thus leading to the control problems. Examination of the strain energy distribution for each of these modes showed that the telescope support structure assembly, principally, and the telescope metering structure, secondarily, contained the majority of the strain energy. In order to reduce the participation in these two modes, one could try to either add damping to the regions of high strain energy or to stiffen up these regions and push the modes out past the control bandwidth. With the geometry of the telescope support structure and the distribution of strain energy in it, it would be difficult to add damping to these modes. Some damping could have been added to these modes based on the strain energy present in the metering structure members through the use of viscoelastically-damped, constrained-layer members, but the performance to weight benefit would have been small due to the (relatively) small amount of strain energy in the metering structure (compared to the telescope support assembly). Thus it was decided to stiffen up both the telescope support assembly and the metering structure to alleviate the participation in the dynamic response caused by these modes. Increasing the section sizes in both of these regions raised the 8.3 and 10.8 Hz modes to 13.6 and 14.7 Hz, respectively. In the end analyses, these changes reduced the problems of closing the control loops by both raising the frequency of the modes and by changing the mode shapes enough to reduce the input-output gain factors.

Strain Energy Analysis and Passive Damping Treatment

"Problem modes" identified in control loop studies examined via strain energy analysis

Two principal modes of concern

- Solar array out-of-plane bending modes near 0.4 Hz
  - Addition of passive joint damper to Solar Array Drive Assembly (SADA) reduced effects of mode
- Telescope support structure and metering truss modes near 8.3 and 10.8 Hz
  - Addition of passive damping deemed not as effective as increasing structural stiffness
  - Stiffening of both the telescope support structure and metering trusses shifted mode frequencies to 13.6 and 14.7 Hz where their effect was reduced by the control loop blending filters

(This page intentionally blank)

Optical Sensitivities

(This page intentionally blank)

(This page intentionally blank)

TRW

Coordinate Frame Definition

The transmit path originates at the transmitter and is split at a dichroic supported by a spider in the BAPTA. Part of the transmitted energy goes to the shot vector sensor, and the remaining energy is reflected off relay mirrors in the BAPTA, through an aperture in the primary mirror, expanded by the secondary mirror and redirected by the primary mirror toward the earth at 45° from the satellite Z-axis which tracks nadir. The nominal (zero strain energy) transmit direction leads the telescope axis and the receive direction lags the telescope axis by a small angle. This is discussed on the following vugraph.

As the optical elements in the transmit and receive paths vibrate, the transmit and receive path directions change.. Since the telescope is canted at 45° relative the satellite Z-axis, there are basically two coordinate systems which facilitate the estimate of the sensitivity of the transmit and receive beam deflections with respect to motion of the optical elements. The first system--the satellite triad, is parallel to the satellite roll, pitch and yaw axes. All modal slope data is given in this system and is also referred to as the global NASTRAN reference. The second system is obtained from the first by rotating the satellite triad -45° about the satellite X-axis. All local-element coordinate systems are parallel to one of the above, with origin located appropriately.

54 55

Coordinate Frame Definition

Two basic coordinate frames are used within which mechanical motion will be given

- Spacecraft frame with origin at the separation plane
- Primary Mirror (PM) frame with origin at the vertex of the PM
- All other mechanical coordinate frames are parallel to one of the above with origin translated appropriately to the optical element or group of optical elements

Spacecraft frame with origin translated to vertex of PM, O_p

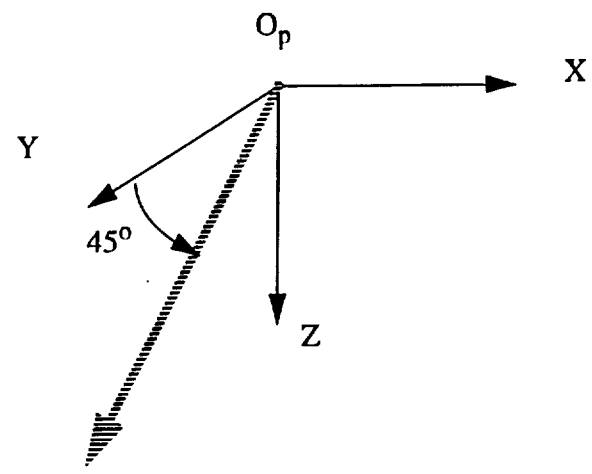

Boresight in YZ-plane for NASTRAN model

Spacecraft frame on PM frame

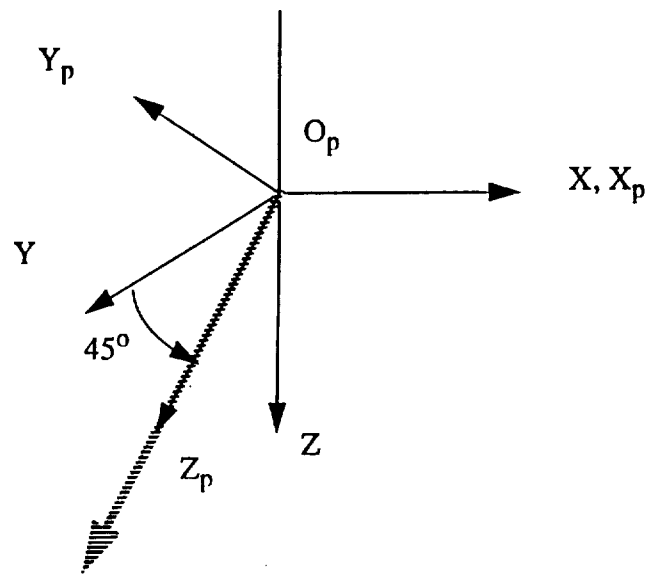

Transmit and Receive Reference Frames

Off-nominal transmit and receive deflections are defined relative the zero strain energy transmit and receive triads. The nominal transmit direction leads the telescope axis, and the nominal receive direction lags the telescope axis. The lead and lag angles are

$$\text{lead/lag angle} = (\text{slant range}/c)\,\omega_{scan}\cos 45^\circ = 0.132 \text{ degrees}$$

TRW has a program for integrating the time-domain dynamics of two flexible bodies moving through large angles relative to each other. For this study, however, the scan motion was not modeled to facilitate the required control loop and strain energy studies.

Transmit and Receive Reference Frames

$S_t = \{X_t, Y_t, Z_t\}$ = transmit (or point ahead) reference

$S_r = \{X_r, Y_r, Z_r\}$ = receive reference

Zero strain energy condition

- Transmit pulse sent in direction Z_t and return pulse (echo) received in direction Z_r

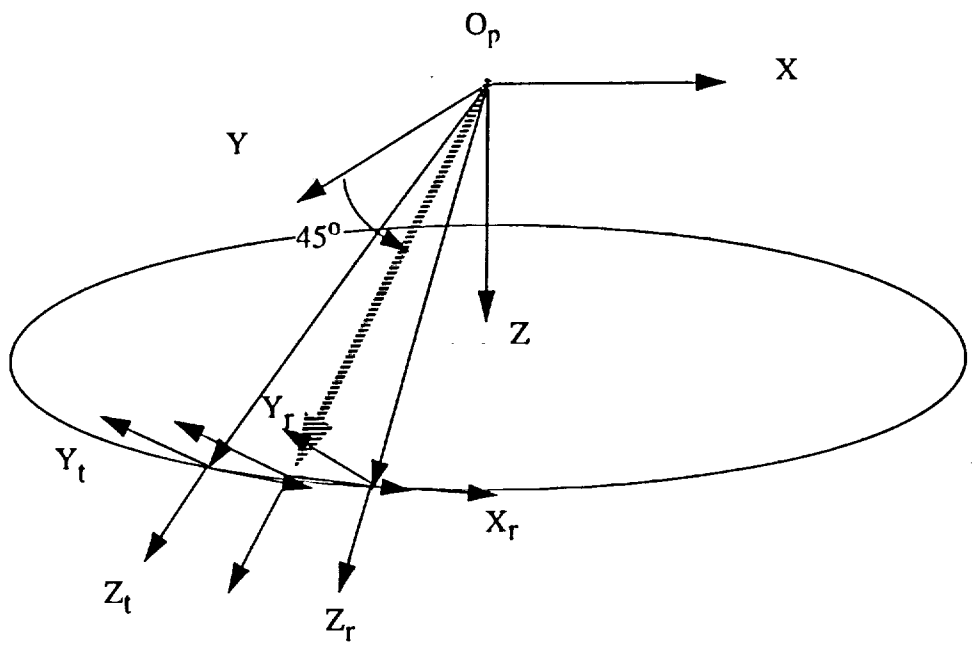

Definition of Transmit and Receive Pointing Errors

The transmit and receive pointing errors are defined relative to the zero strain energy reference frames as shown. Deflections along X and Y correspond to rotations about the X and Y axes, respectively.

Optical sensitivities (discussed on the next vugraph) are computed for the major optical elements; the primary mirror, the LED, the secondary mirror, the relay optics in the BAPTA, the transmitter/receiver assembly, and the optical bench. The relay optics consist of relay mirrors.

Definition of Transmit & Receive Pointing Errors

Motion of optical elements in transmit path will cause an equivalent (zero strain energy) deflection of transmit pulse as defined relative to reference S_t

Similarly, motion of optical elements in receive path will cause error at receiver equivalent to a return pulse error as defined relative to the reference S_r

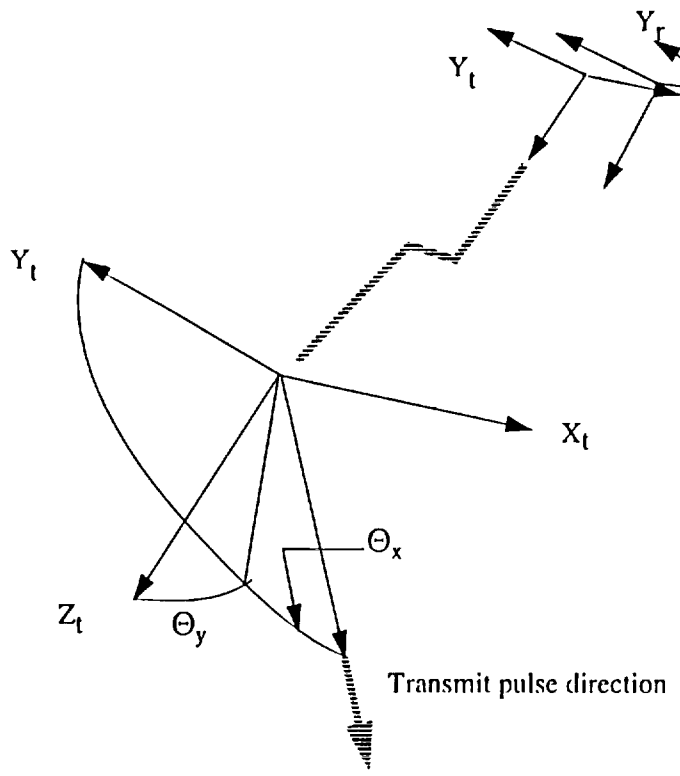

Transmit pulse direction

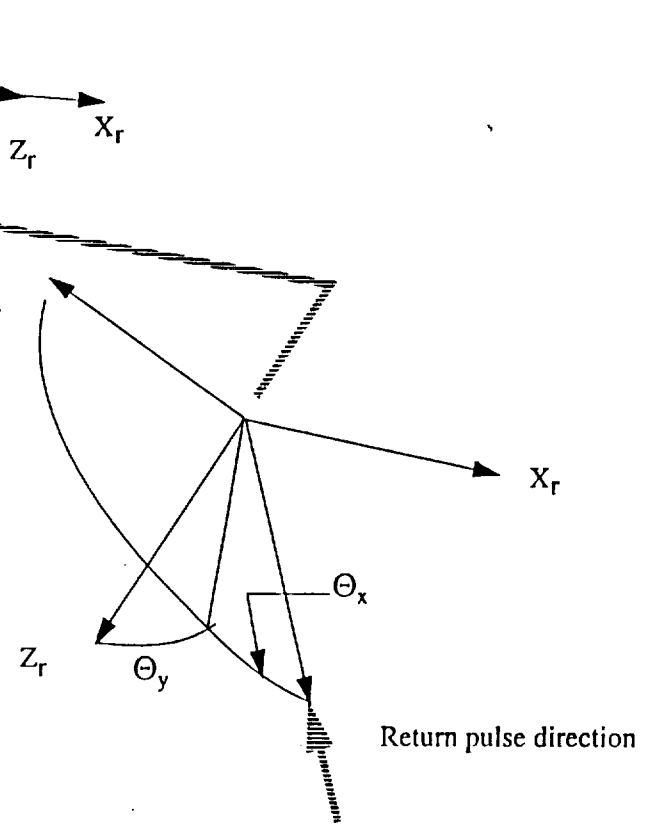

Return pulse direction

Primary Mirror Optical Sensitivity Coefficients

The primary mirror (PM) optical sensitivities are non-zero only for rotations about and displacements perpendicular to the PM symmetry axis, as indicated by the bolded boxes in the table below.

Displacements of the PM are equivalent to rotations of the far-field source direction which is equal to the PM physical displacement divided by it focal length. The displacement sensitivities are therefore 15.7 mrad (far-field) per inch displacement.

For the rotational optical sensitivity of the PM, a rotation of the PM about the X-axis by a small angle, δ, is equivalent to returning the strain energy to zero and moving the far-field source by 2δ about the same axis. The PM rotational optical sensitivity is then 2 μrad (far-field)/μrad (local rotation).

Primary Mirror Optical Sensitivity Coefficients

S_p denotes reference frame $\{X_p,Y_p,Z_p\}$ with origin at the vertex of primary mirror

Rotations and deflections of the primary mirror in S_p will cause deflections of the incoming beam at the entrance aperture of the optical bench

Optical sensitivity coefficients are defined by equivalent far-field deflections about X_t, Y_t axes (and the X_r,Y_r axes) divided by the motion of the primary mirror

PM Optical Sensitivity Coefficients

	X_p Displacement	Y_p Displacement	Z_p Displacement	X_p Rotation	Y_p Rotation	Z_p Rotation
Θ_x Sensitivity	$\frac{\partial\Theta_x}{\partial x_p}$	$\frac{\partial\Theta_x}{\partial y_p}$	$\frac{\partial\Theta_x}{\partial z_p}$	$\frac{\partial\Theta_x}{\partial\Theta_{px}}$	$\frac{\partial\Theta_x}{\partial\Theta_{py}}$	$\frac{\partial\Theta_x}{\partial\Theta_{pz}}$
Θ_y Sensitivity	$\frac{\partial\Theta_y}{\partial x_p}$	$\frac{\partial\Theta_y}{\partial y_p}$	$\frac{\partial\Theta_y}{\partial z_p}$	$\frac{\partial\Theta_y}{\partial\Theta_{px}}$	$\frac{\partial\Theta_y}{\partial\Theta_{py}}$	$\frac{\partial\Theta_y}{\partial\Theta_{pz}}$

Coefficients in dark border are the only non-zero coefficients for the primary mirror

(This page intentionally blank)

Disturbance Models

(This page intentionally blank)

(This page intentionally blank)

Receiver Jitter Control

The pulse frequency of the 2 μm LAWS system is 4.7 Hz on average. The scan frequency is 12 rpm or 0.2 Hz and 22 laser pulses are sent and received each scan. At an altitude of 525 km and a slant range of 776 km, the pulse echo is received in 5.2 msec and is broadened by the round trip time through the atmosphere to ≈ 200 μsec. Jitter at the receiver is controlled using two fast steering mirrors (FSMs), as shown in the figure, which position the return pulse on the receiver and maintain it there for the broadened pulse width.

The receiver jitter control problem consists of 1) correcting for the structural vibrations induced in the transmit and receive paths by the disturbances within the payload and on the satellite bus; 2) correcting for the line-of-sight (LOS) inertial change during the pulse echo caused by ephemeris changes and the scan angle change; and 3) correcting for the transmitter jitter using the shot vector sensor data.

This study is directed at correcting for the structural vibrations induced in the transmit and receive paths by disturbances and displacement-energy sources in the payload and spacecraft. It was assumed in the study that the laser transmitter/receiver assembly, the transfer optics and the primary mirror, itself, were rigid bodies. The spacecraft, payload support structure, primary mirror reaction structure, scan bearing (BAPTA) and solar arrays were modeled as flexible bodies. Relative motions between the various elements are indicated by the first bending mode stiffnesses shown on the vugraph.

Clearly, if the transmitter and receiver are located in relative close proximity, then estimating the inertial attitude change of the LED on the primary mirror over 5.2 msec and nulling the relative alignment between the LED and the boresight sensor (BS) would be adequate up to the non-common optical jitter. Thus, we null the BS signal using the FSM and command the LAFSM with the signals

$$\Delta\Theta_x = \int_{t_p}^{t} \hat{\omega}_x(\xi)d\xi$$

and

$$\Delta\Theta_y = \int_{t_p}^{t} \hat{\omega}_y(\xi)d\xi$$

where $\hat{\omega}_x$ and $\hat{\omega}_y$ are the LED inertial rate estimates orthogonal to the boresight. The integration is from t_p to t where t_p is the time of the transmit pulse and $(t-t_p)$ is at least 5.2 msec. The above integrals are correct for this study which does not model the point ahead optics for the transmit pulse nor the lag optics in the receive path. In reality, the LED inertial estimate $\hat{\omega}_y$ has a scan rate component which, when integrated over the nominal echo time, is compensated by the difference between the transmit and receive optical paths.

Receiver Jitter Control

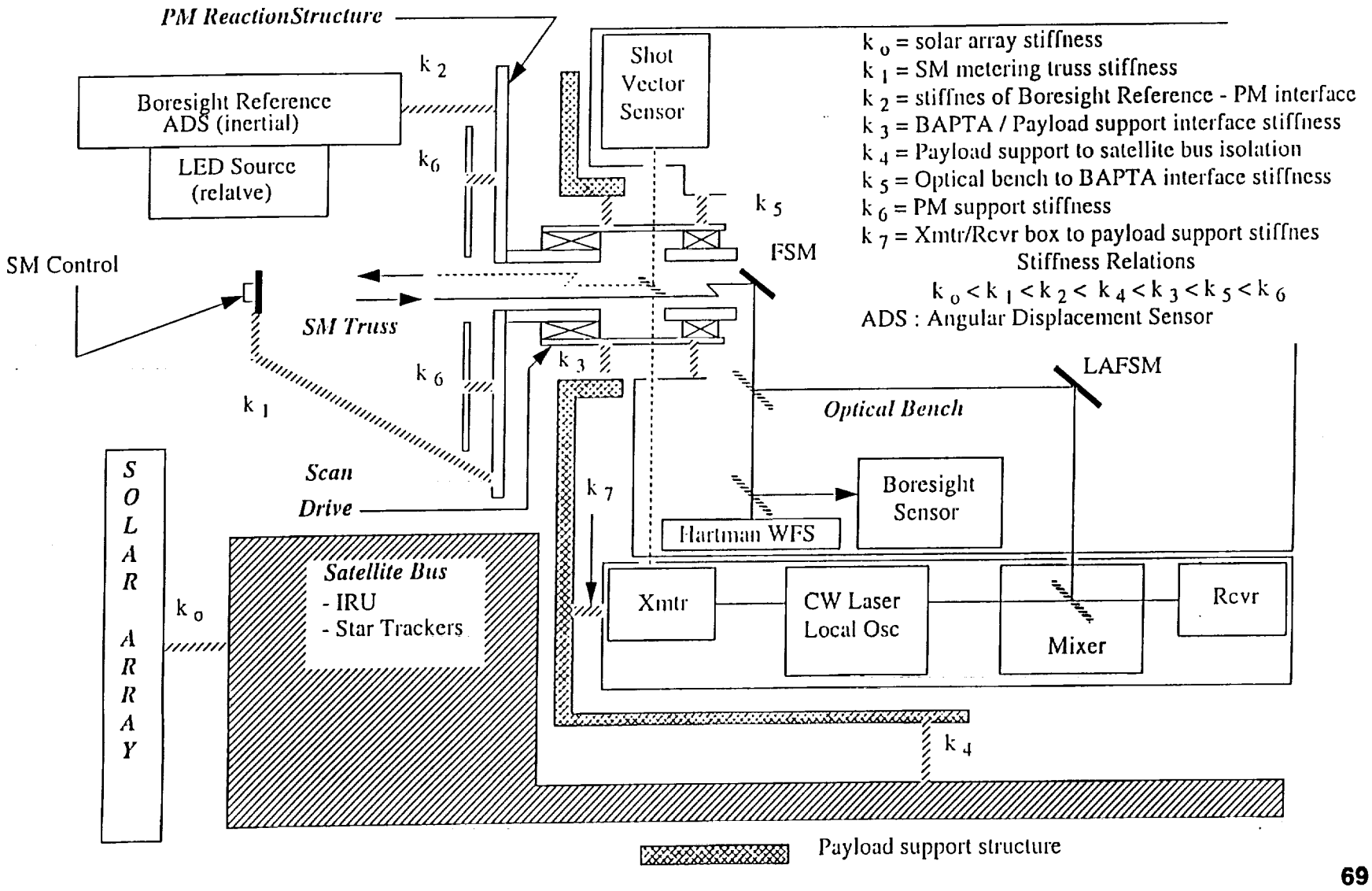

k_0 = solar array stiffness
k_1 = SM metering truss stiffness
k_2 = stiffnes of Boresight Reference - PM interface
k_3 = BAPTA / Payload support interface stiffness
k_4 = Payload support to satellite bus isolation
k_5 = Optical bench to BAPTA interface stiffness
k_6 = PM support stiffness
k_7 = Xmtr/Rcvr box to payload support stiffnes

Stiffness Relations

$k_0 < k_1 < k_2 < k_4 < k_3 < k_5 < k_6$

ADS : Angular Displacement Sensor

Reaction Wheel Loop

The reaction wheel torque noise is derived for the modified Teldix RDR-68 (68 nms @ 6000 rpm). This reaction wheel is currently recommended for the Advanced X-ray Astrophysics Facility - Imaging (AXAF-I) being built at TRW. The angular momentum for the AXAF-I mission will be increased from 68 nms to 81 nms, and the torque capability will be 0.14 nm (20 in-oz).

The reaction wheel assembly (RWA) consists of five subassemblies: 1) Housing, 2) Flywheel, 3) Ball bearing unit, 4) Motor rotor, and 5) Commutation electronics with motor stator.

The reaction wheel drive electronics assembly (RWDEA) in a simplified sense receives power from the satellite power bus, drives the three-phase, 8-pole motor, receives commutation signals from RWA which are processed in the commutation logic and the tach processing logic.

The tachometer data is sent to the onboard computer (OBC) upon request every 256 msec and is used to estimate the RW momentum. Torque commands from the satellite main body controller with bending filters (discussed later) are multiplied by -1 and integrated to give the desired RW momentum. The momentum error is processed by a PI (proportional-integral) controller to give the command torque which is formatted as a digital word and sent to the RWDEA. The digital word formatting is represented mathematically as a quantizer. The torque command quantization is 0.001 nt-m.

The tachometer can be operated in two modes: 1) the pulse interval mode, or 2) the pulse count mode. Each count indicates a wheel rotation of 7.5°. The pulse interval mode uses a 64 kHz clock to measure the time between pulses. When a tach request is received, the most recent time interval is sent. In the pulse count mode, the number of pulses in a fixed time interval, usually the OBC minor cycle, are counted. The pulse count mode was simulated for this study.

The commanded torque is integrated to give wheel rate. The wheel rate is integrated over one OBC minor cycle or 256 msec, added to the fractional pulse in radians previously uncounted, quantized in counts, and placed in a buffer awaiting OBC request. All parameters of the reaction wheel loop are given in the table on the figure.

Reaction Wheel Loop

Reaction wheel loop definition

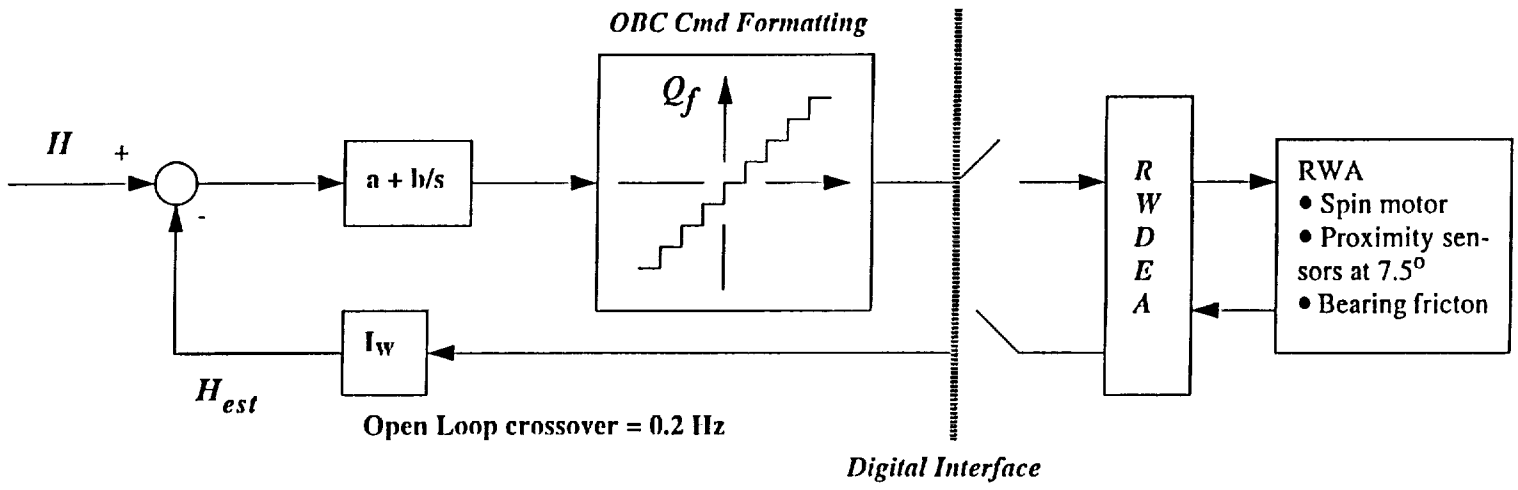

Reaction Wheel Loop Parameters

Mnemonic	Description	Units	Value
a	Proporational gain	rad/sec	2.29
b	Integral gain	rad/sec^2	0.654
q_f	Equivalent torque cmd quantization	nt-m	0.001
I_w	Reaction wheel inertia	nt-m-sec^2	0.18023
q	Reaction wheel positional quantization	rad	$7.5^o x \pi/180^o$
T_s	Minor cycle sample period	sec	0.256
s_f	Tachometer scale factor	rad/cnt-sec	0.511327

Reaction Wheel Loop Simulation Diagram

TRW

The simulation diagram representing the reaction wheel control loop discussed on the previous vugraph is shown here.

Reaction Wheel Loop Simulation Diagram

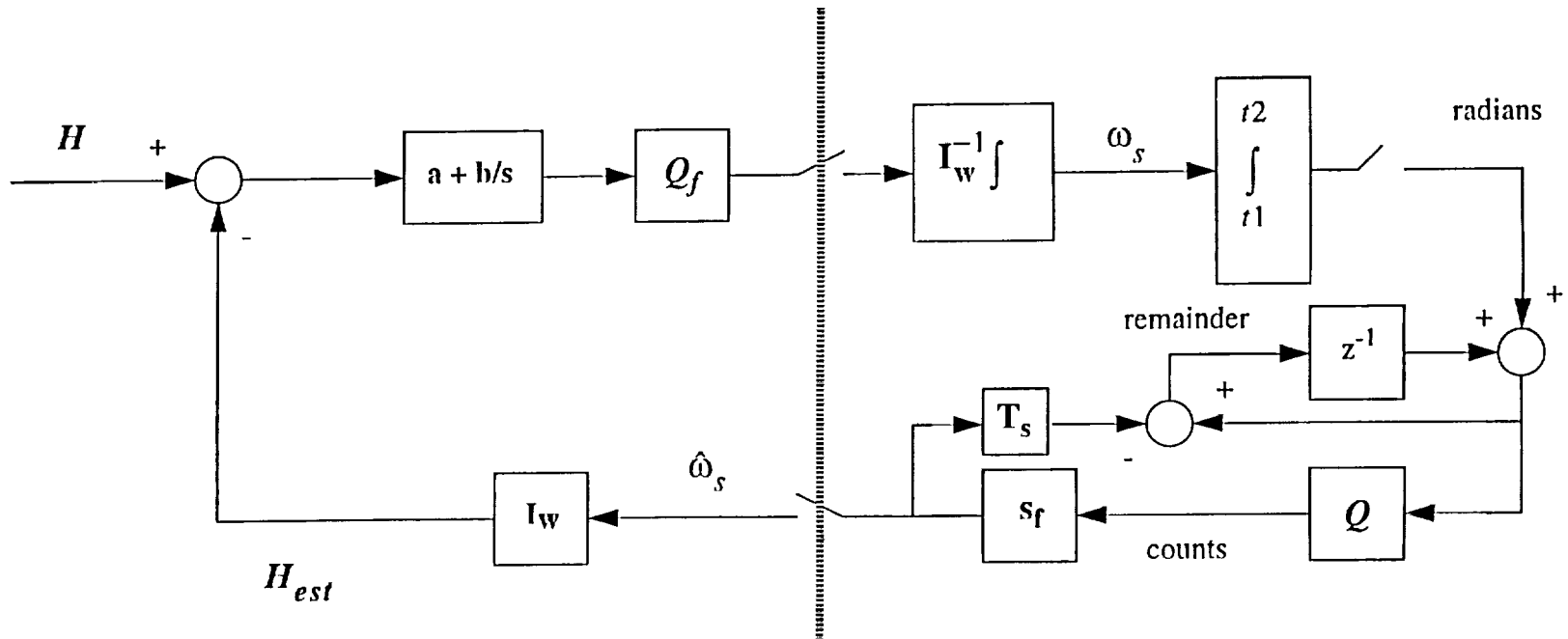

Digital Interface

Torque Noise Examples

The momentum loop open-loop crossover is set at 0.2 Hz for an anticipated satellite main body loop of 0.02 Hz. To get the torque noise, a sinusoidal momentum command at orbit rate is used. The momentum command for this example is

$$h_{cmd}(t) = 12\sin(\omega_o t - \pi/4) \quad \text{nt-m-sec}$$

The reaction wheel spin speed estimate is plotted against the true spin speed. This estimate causes a similar variation in the estimated momentum which ripples through the OBC software to cause an eventual variation in the torque out of the spin motor. The torque noise is computed as the spin motor torque minus the time derivative of the momentum command.

Torque Noise Examples

Torque noise examples without reaction wheel bearing friction, spin motor time constant, or pulse width modulated (PWM) wheel drive

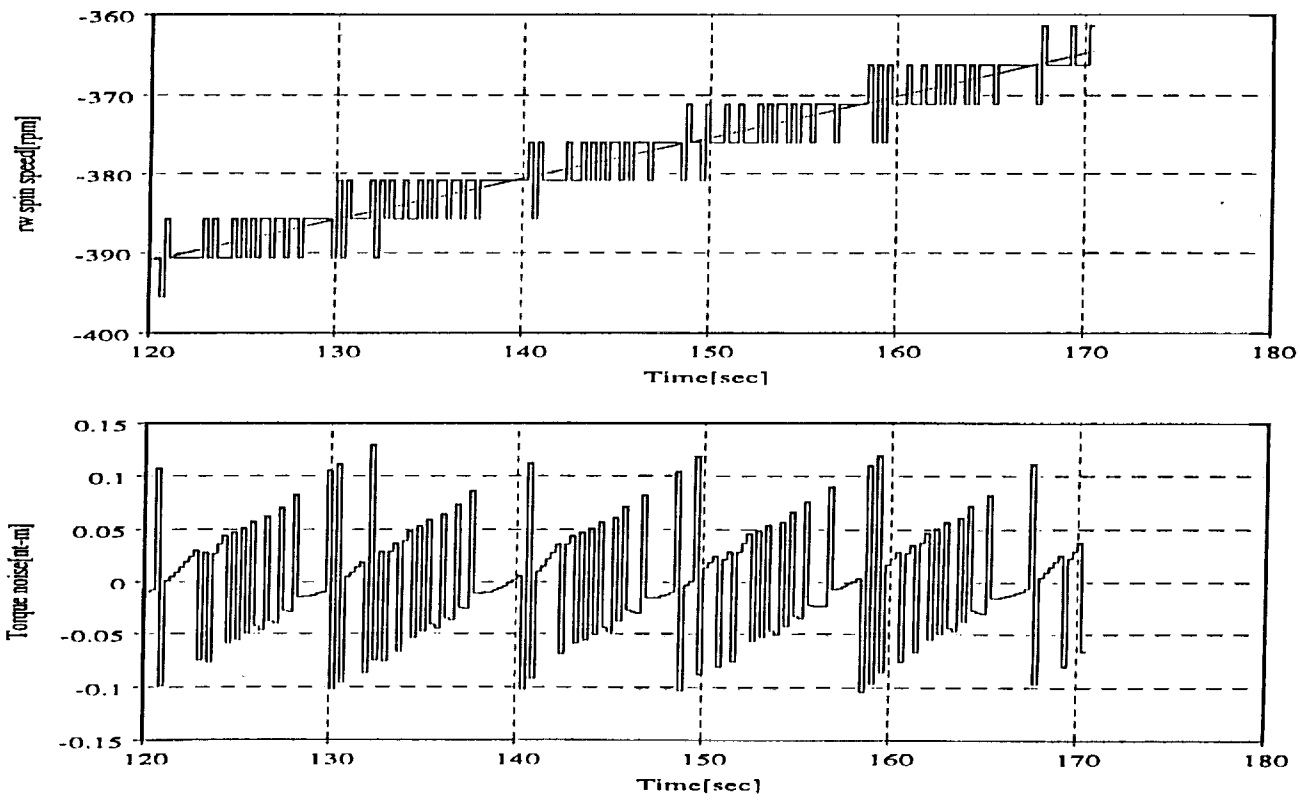

Reaction Wheel Torque Noise

Changing the amplitude of the momentum command changes the frequency content of the torque noise. The maximum frequency is governed by the OBC minor cycle and is approximately 4 Hz. The torque noise (1σ) is

$$\sigma = 0.707 \times 0.1 \times 8.85 = 0.625 \text{ in-lbs}$$

Assuming a constant PSD level from 0.01 Hz to 4 Hz, allowing the PSD to ramp up 40 dB per decade to 0.01 Hz and fall off 40 dB per decade after 4 Hz, the level k of the plateau for a one-sided PSD is

$$k = \left(\frac{\sigma^2}{2\left(4 - \frac{0.01}{3}\right)} \right) = 0.049 \quad (\text{in-lb})^2/\text{Hz}$$

As a point of clarity, a one-sided PSD S(f) means

$$\sigma^2 = \int_0^\infty S(f)df$$

Reaction Wheel Torque Noise

Reaction wheel torque noise frequency content changes as the command momentum changes

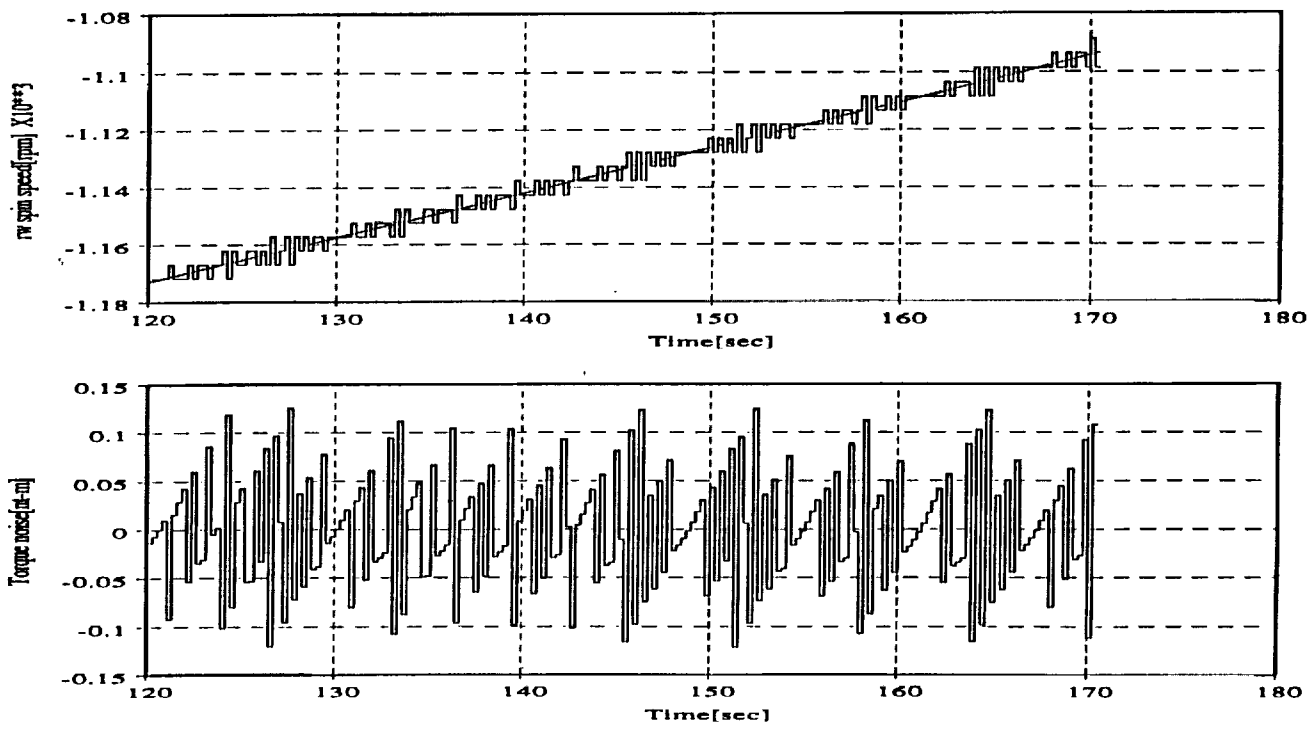

Receiver Open Loop Jitter

The receiver jitter measured relative to a source in inertial space is 4.3 μrad (1σ), far-field, about the X-axis and 5.8 μrad (1σ), far-field, about the Y-axis. The X and Y axes are the receiver axes projected to output space as discussed in the section on Optical Sensitivities. The structural damping is 0.5 percent. To check the sensitivity to damping, the time simulation used a structural damping of 0.2% The 1σ jitter is inversely proportional to the square root of the damping. Thus the expected jitter about the X and Y axes, respectively, is

$$4.3 \times (5/2)^{1/2}\ \mu\text{rad} \rightarrow 6.8\ \mu\text{rad}$$

and

$$5.8 \times (5/2)^{1/2}\ \mu\text{rad} \rightarrow 9.2\ \mu\text{rad}$$

which compares favorably with the time simulation shown on the following vugraph.

Receiver Open Loop Jitter

Estimated receiver open loop jitter relative to a source in inertial space from three orthogonal reaction wheels is less than 6 µrad per axis. Damping in structural model is 0.5 percent

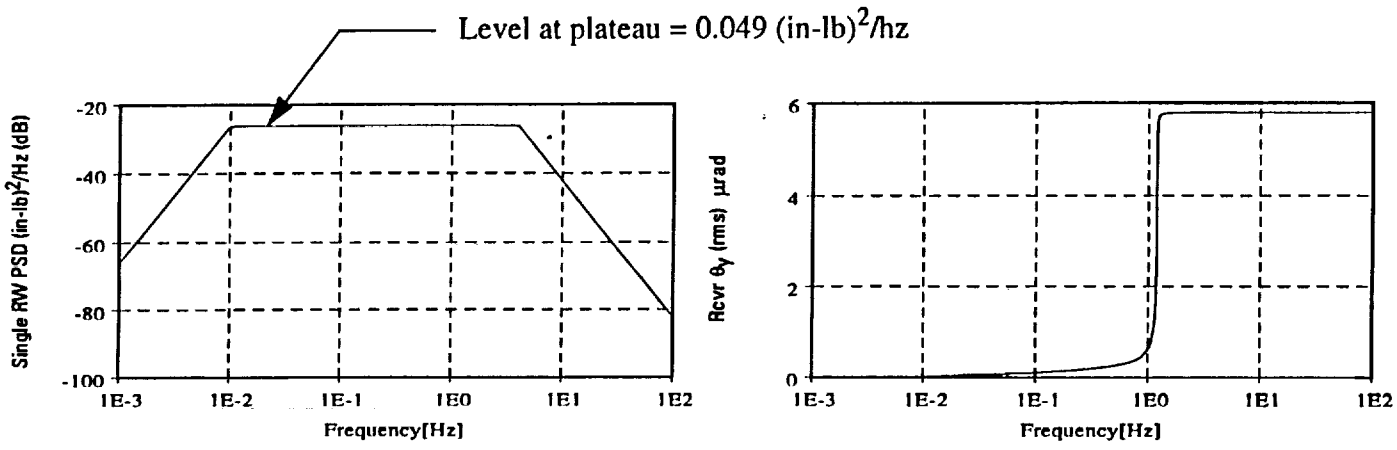

Table 1: RMS Rcvr Jitter from 3 RWs

Θxp(µ-rad)	Θyp(µ-rad)
4.3	5.8

Open Loop Receiver Response

In actuality, the receiver signal measures the change in the structural bending between the transmit pulse and the received pulse echo ≈ 5 msec later. The receiver and transmitter are located on the optical bench which was modeled as a lumped mass and inertia. In this study, the transmitter and receiver have the same effective slopes (defined by the optical sensitivities integrated against the NASTRAN modal slopes at distinct optical elements).

The jitter about the X-axis is primarily at 0.42 Hz and the jitter about the Y-axis is primarily at 1.12 Hz. The estimated receiver signals about the X and Y axes, respectively, are

$$6.8 \times 2\sin(\pi \times 0.42 \times 0.005)\ \mu\text{rad} = 0.09\ \mu\text{rad}$$

and

$$9.2 \times 2\sin(\pi \times 1.12 \times 0.005)\ \mu\text{rad} = 0.32\ \mu\text{rad}$$

Open Loop Receiver Response

Open loop receiver response with all main body loops closed and reaction wheel disturbances acting on satellite. Damping in structural model is 0.2 percent

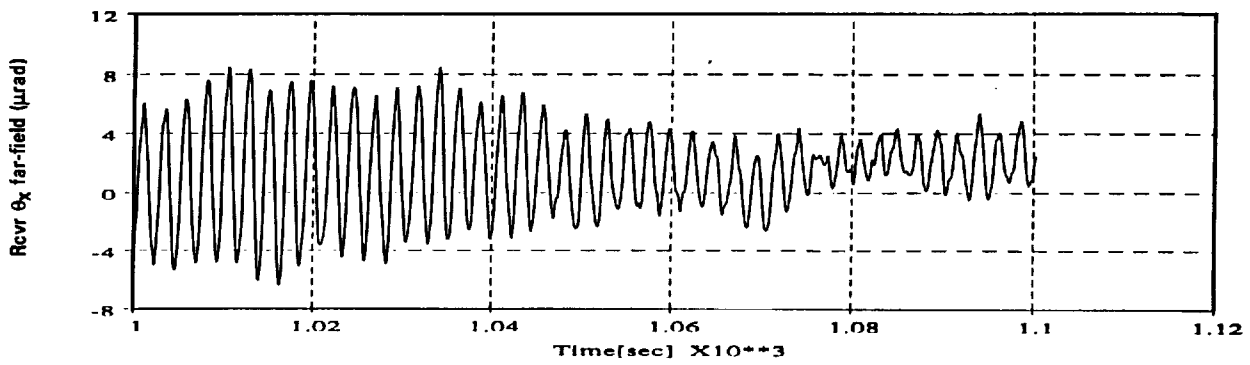

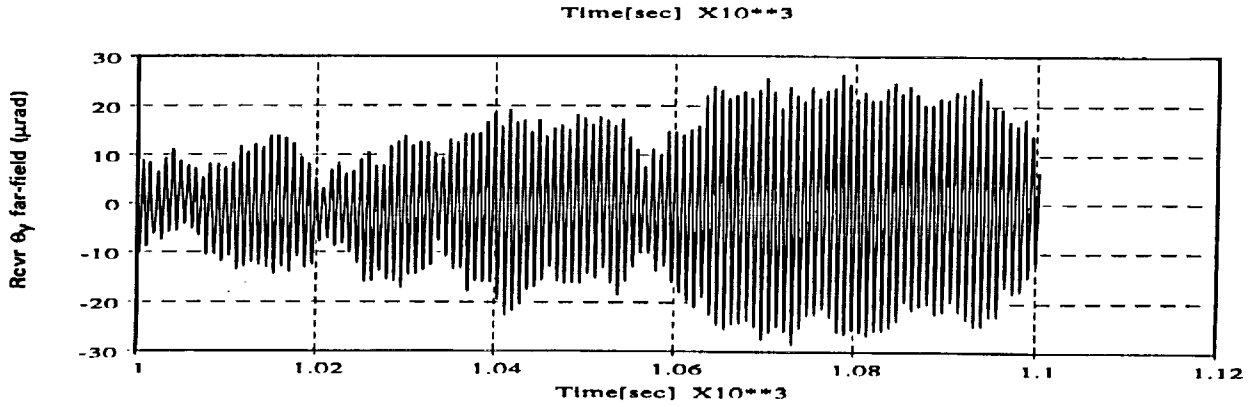

Open Loop Receiver Response - II

The open loop receiver response relative to the transmitted pulse launched 5 msec earlier is shown here.

Open Loop Receiver Response - II

Open loop receiver response relative to pulse transmitted 5 ms earlier. All main body loops closed and reaction wheel disturbances acting on satellite. Structural damping at 0.2 percent

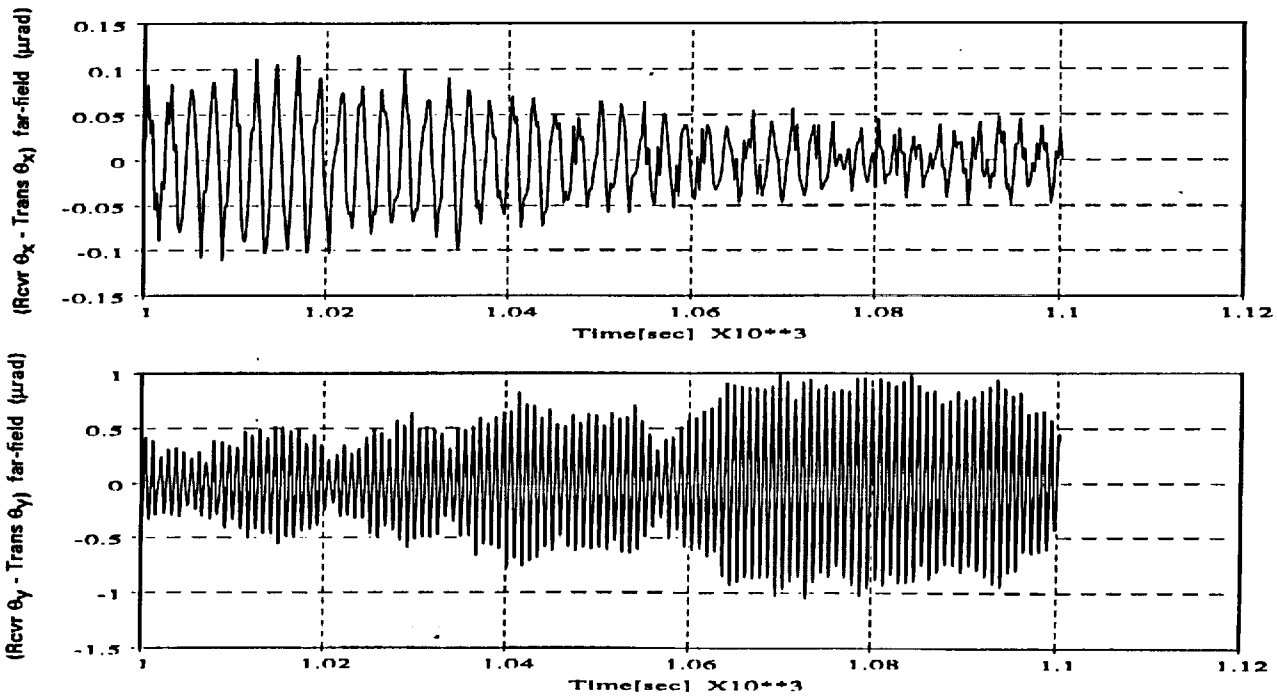

Open Loop Boresight Response

The boresight sensor signal is computed by fixing a source to the primary mirror at the LED location. Thus, this source now moves in accordance with the primary mirror LED/ADS structural node. The boresight signals are an attenuated version of the receiver signals since the boresight sensor (BS) measures the relative alignment between the LED and the BS on the optical bench.

Open Loop Boresight Response

Open loop boresight sensor response with all main body loops closed and reaction wheel disturbances acting on satellite

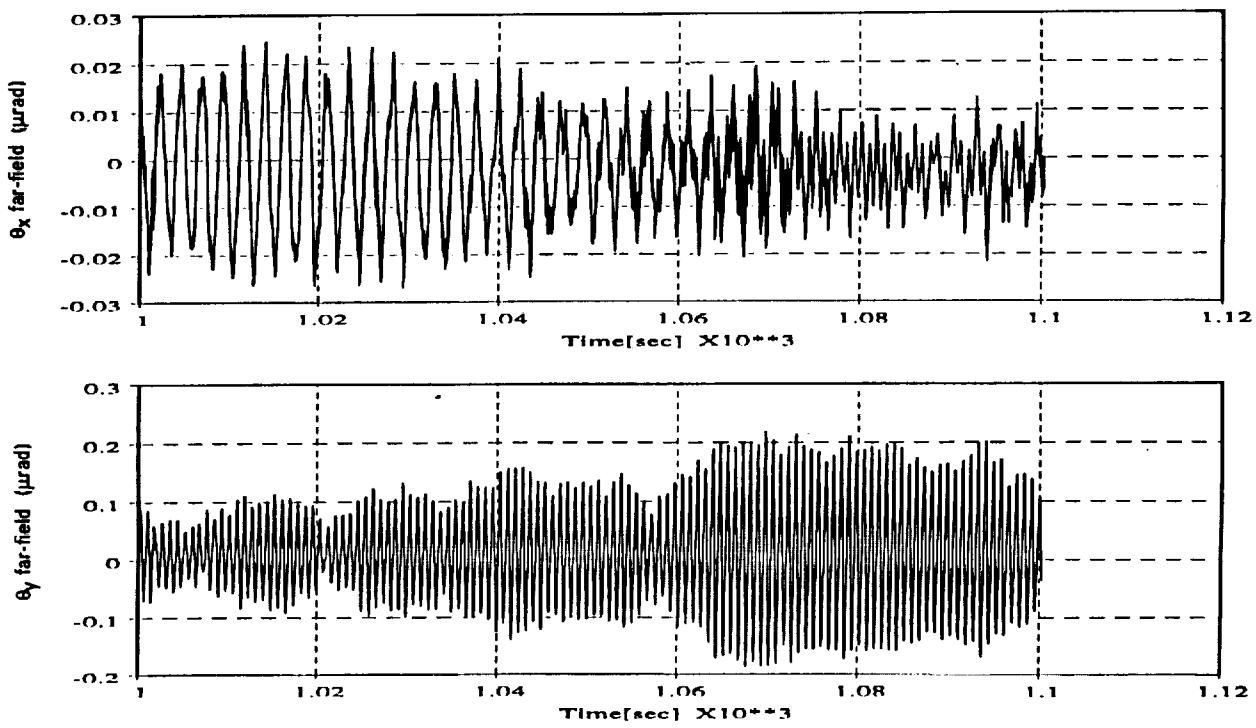

Structural Transmission from Reaction Wheel to Receiver

To check the dominant modes, the structural transmission from the reaction wheel to the receiver jitter relative to an inertial source was computed. The structural model used has a single grid point for the reaction wheel assembly. From the transfer function, the dominant bending mode for the receiver X rotation is at 0.42 Hz. The dominant bending mode for the receiver Y rotation is at 1.12 Hz.

Structural Transmission from Reaction Wheel to Receiver

Transfer functions for reaction wheels to receiver relative to inertial source

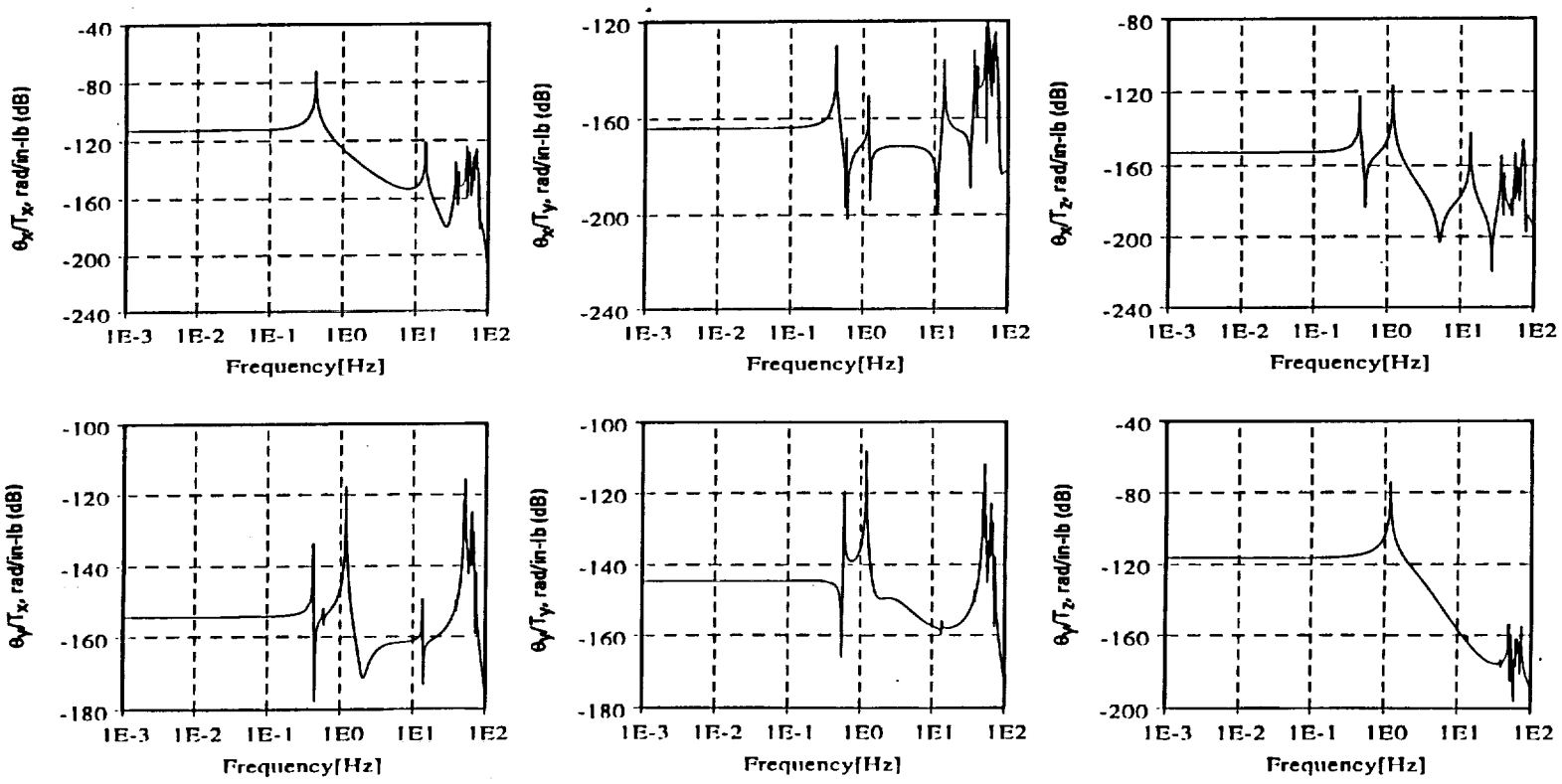

Solar Array Drive Assembly Induced Disturbances

The only solar array disturbances included in this study originate at the two SADAs. The array is representative of the Fokker panel array taken from TRW's TDRS-Flight 7 model. It is our understanding that thermal loading on a preloaded blanket array for a satellite having just come out of eclipse will cause the array to move from one equilibrium configuration to another through a jump discontinuity. The Fokker panel array has more thermal mass than an equivalent size blanket array under preload; thus, there is no thermal snap problem anticipated for the Fokker arrays.

The SADA is a stepper with a 101:1 harmonic drive. The cardinal step is 0.015°. The two SADAs are synchronously commanded in an open loop fashion every 256 msec. The equivalent drive stiffness, in torsion, is 100,000 in-lb/rad. The +Y SADA disturbance is modeled as the difference between the continuous ramp $\omega_0 t$ and the quantizing ramp acting through the drive stiffness on the outboard structural node. An equal and opposite reaction torque acts on the inboard node. The =Y SADA experiences the same action/reaction torques.

Solar Array Drive Assembly Induced Disturbances

There are two solar array wings each driven with an independent solar array drive assembly (SADA)

Each SADA is basically a stepper with a 101:1 harmonic drive

The cardinal step is 0.015 degrees

Each SADA is commanded in an open loop fashion based on the satellite and sun ephemerides

The disturbance generated at ±Y SADAs is given by the following

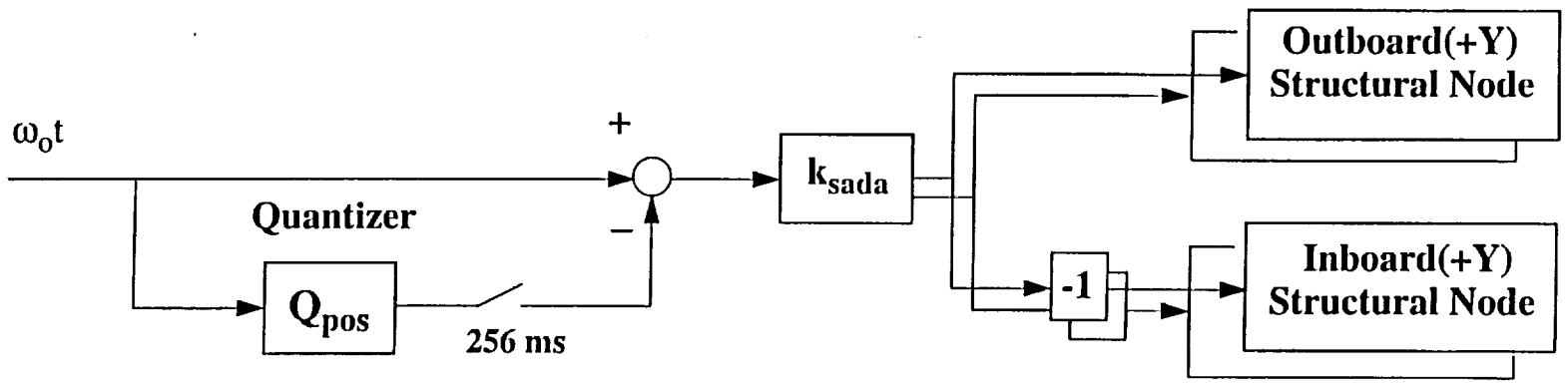

K_{sada} = 100,000 in-lb/rad
q_{pos} = 0.015 deg

Open Loop Receiver Response to SADA Disturbances

The SADA disturbances produce an open-loop jitter at the receiver relative to the transmitter LOS delayed ≈ 5 msec. The solar arrays are gimbaled about the satellite Y-axis and the disturbance response about the orthogonal X-axis is only 4 to 5 nrad. The disturbance response about the Y_p direction (orthogonal to the nominal receive direction) is ≈ 230 nrad. The responses were estimated by turning off the scan bearing disturbances and letting the reaction wheel command torques, as computed in the OBC, following the bending-mode filtering act directly on the satellite.

Open Loop Receiver Response to SADA Disturbances

Open loop receiver response to SADA disturbances relative to a transmitted pulse 5 ms earlier

- Estimated in the time domain by taking the command torque from the satellite main body controller after bending mode filtering and allowing it to act on the satellite, thus bypassing the three reaction wheel models

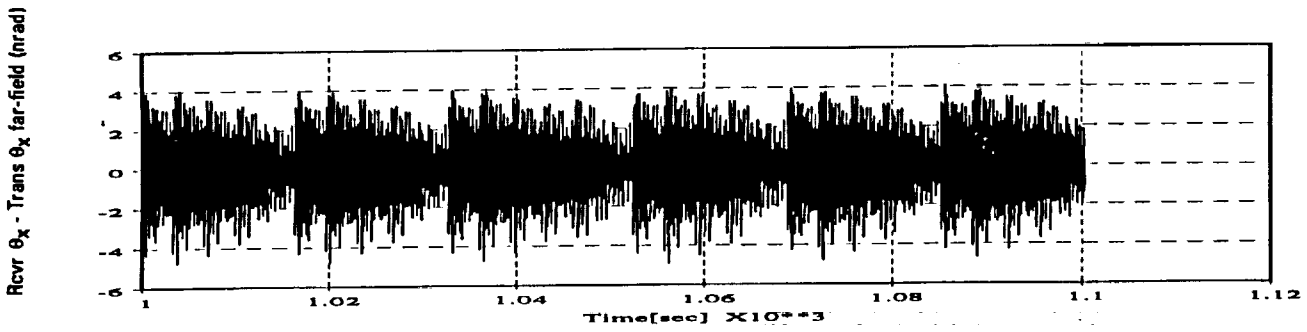

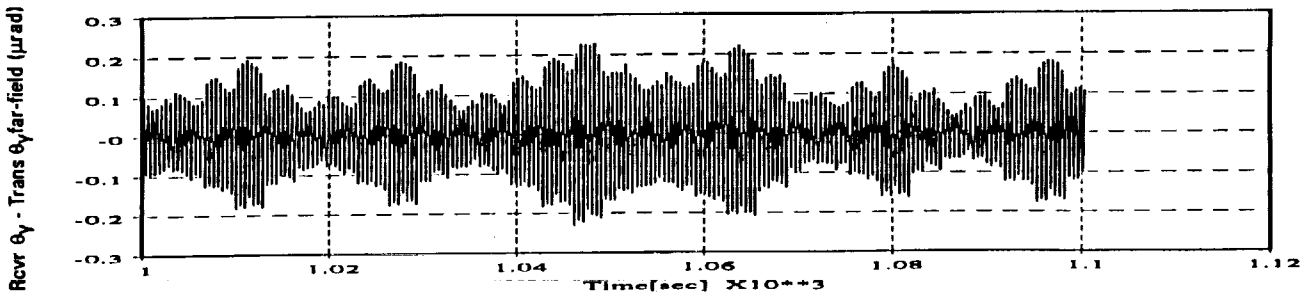

Bearing & Power Transfer Assembly (BAPTA) Summary

The scan bearing (BAPTA) mechanism consists of a duplex pair of bearings. To measure the pointing errors introduced by this mechanism, the complete BAPTA, without telescope, is placed in a test fixture. The BAPTA satellite interface is tied to ground, and a reflective flat is fixed to the base of the scan motor rotor. An autocollimator is used to project a collimated source toward the flat. The reflected beam tracks twice the bearing error which changes as the rotor is moved in azimuth. The bearings produce scan axis errors that can be grouped as:

- Misalignment....generates dc and 1st harmonic pointing error
- Radial runout....generates slight variation in the 1st harmonic and additional harmonics
- Non-repeatable runout....generates random motion

The estimated bearing test data for a 14 inch BAPTA is shown in the table on the vugraph.

Bearing & Power Transfer Assembly (BAPTA) Summary

Bearing Geometry

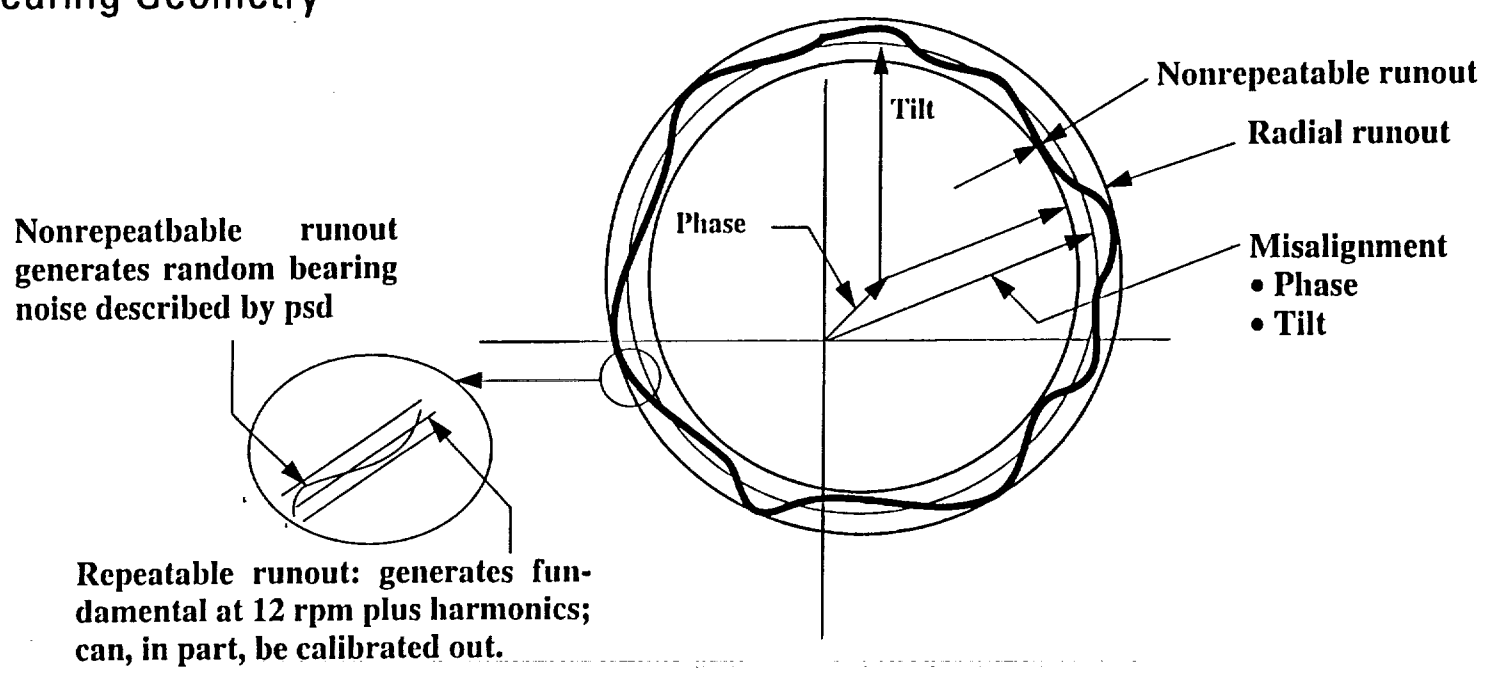

Estimated Bearing Test Data for 14 Inch BAPTA

Error	Value	Comments	Pointing Error
Phase	Calibratable	dc misalignment component	
Tilt	Calibratable	Misalignment fundamental	
Repeatable runout	0.0004" (p-p)	Mechanically non-correctable	6.3 arc sec
Nonrepeatable($dr/d\phi$)	0.0001"(p-p)/30° segment	Ball mismatch and race waviness	0.6 arc sec

BAPTA Induced Disturbances

The BAPTA interfaces with the satellite and telescope assembly at different locations. The satellite interface nodes are averaged in azimuth to define an equivalent inboard structural node. Similarly, the telescope modal data at the telescope assembly interface nodes are averaged in azimuth to define an equivalent outboard structural node. The stiffness between these two nodes corresponds to the stiffness between the two interface points.

The bearing torque disturbance is computed by taking the spectral representation of the rotational noise about the two axes orthogonal to the scan drive, multiplying the stiffness between the interface points, and driving the structure at the interface points with action, reaction torques, respectively.

BAPTA Induced Disturbances

Estimated bearing test data assumes BAPTA scan mechanism effectively tied to ground in a test fixture. An autocollimator projects a collimated source toward a flat on the base of the scan motor rotor. The reflected beam tracks twice the bearing error which changes as the rotor is moved in azimuth

Taking test data to a free-free satellite LAWS payload is accomplished by putting action and reaction torques on the outboard and inboard equivalent nodes in the structural model

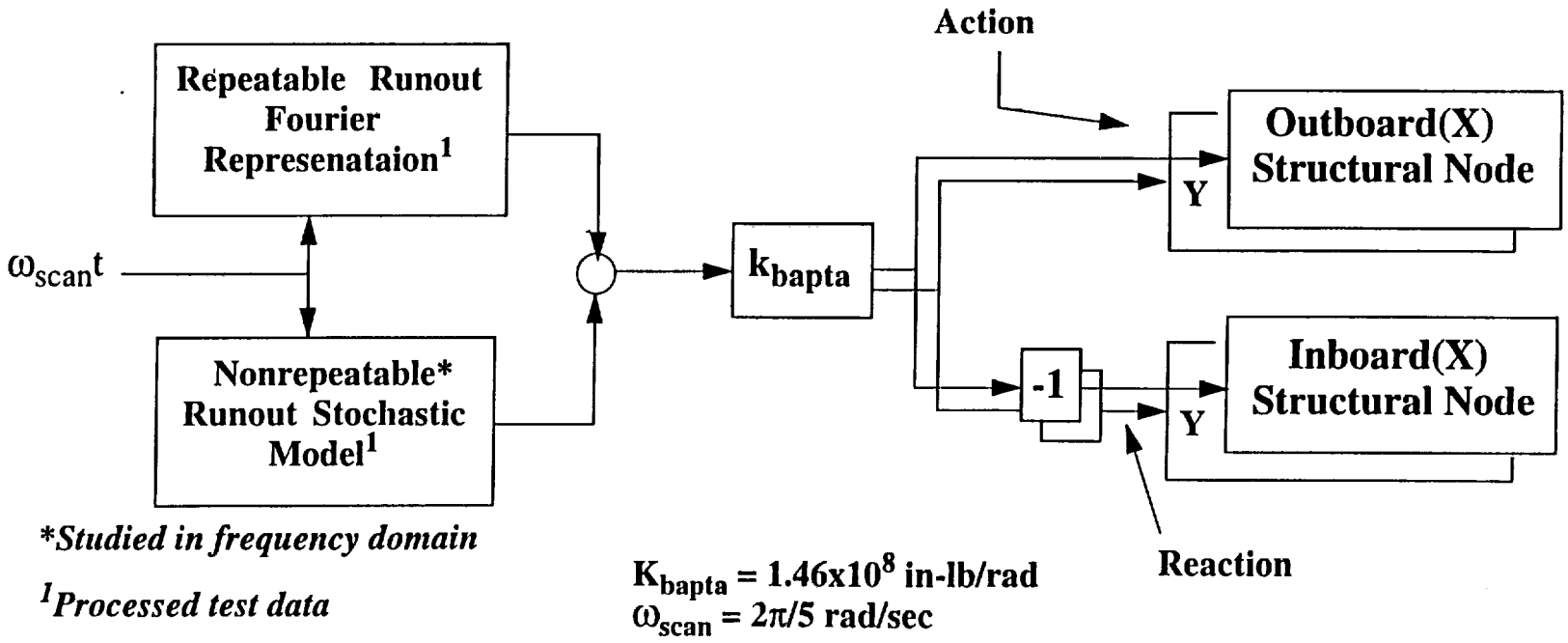

*Studied in frequency domain

[1]Processed test data

$K_{bapta} = 1.46x10^8$ in-lb/rad

$\omega_{scan} = 2\pi/5$ rad/sec

Open Loop Receiver Response to BAPTA Disturbances

The open loop receiver jitter is computed by taking the receiver LOS at time, t, and subtracting the transmitter LOS 5 msec earlier. The SADA and reaction wheel disturbances are set to zero. The random bearing disturbance; thus, the excitation of the structural mode at 13 Hz is not present in these time histories.

For the first three harmonics in the repeatable runout, the LOS motion about the X axis is ≈ 35 nrad. The LOS motion about Y_p is ≈ 80 nrad.

Open Loop Receiver Response to BAPTA Disturbances

Open loop receiver response to BAPTA disturbances relative to a pulse transmitted 5 ms earlier

- Estimated in the time domain by taking the command torque from the satellite main body controller after bending mode filtering and allowing it to act on the satellite, thus bypassing the three reaction wheel models. Only the first three harmonics in the repeatable runout were used

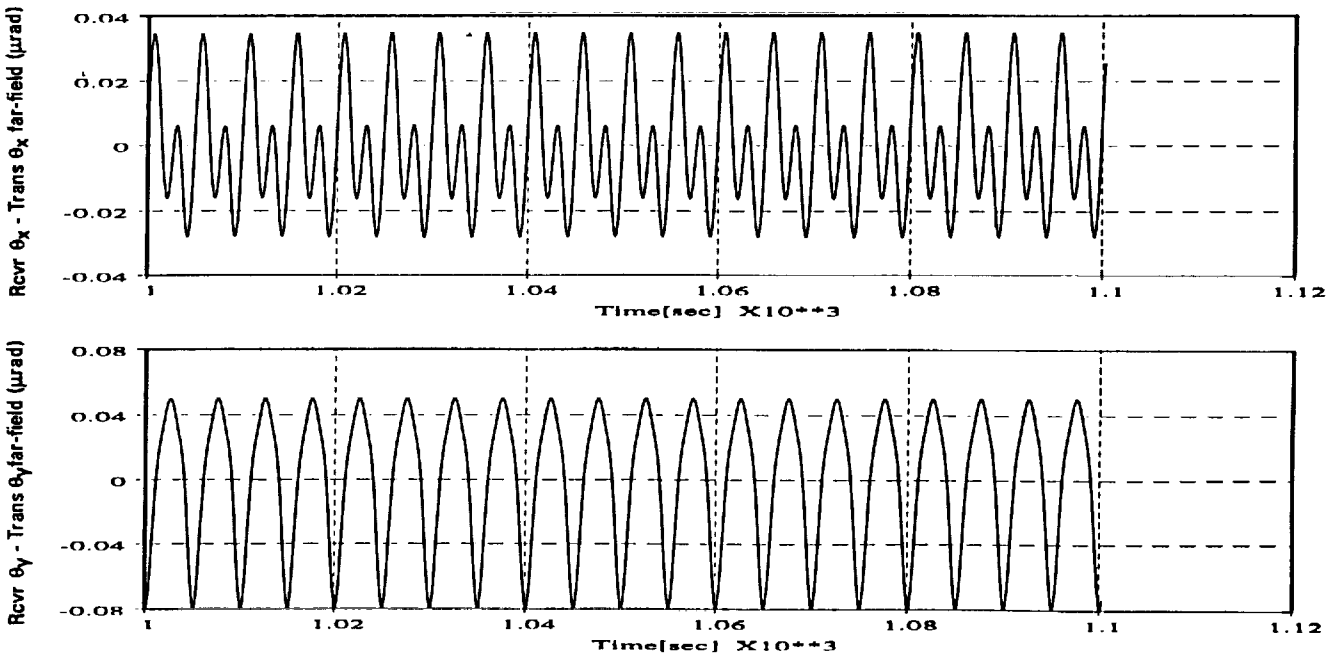

(This page intentionally blank)

Boresight Jitter and Receive Path Control Open Loop Time Domain Response

(This page intentionally blank)

(This page intentionally blank)

Time and Frequency Domain Analyses

The approach taken in the time and frequency domain analyses which follow is summarized on the following two vugraphs.

Time and Frequency Domain Analyses

Studies performed in three axes

Studies focus on two distinct aspects of problem

- Performance in lab setting where receiver jitter is measured for a fixed inertial source in the lab
- Performance on orbit where the receiver jitter is actually the difference between the receiver LOS and transmit LOS 5 msec earlier

Frequency Domain studies performed include

- Blending of IRU, ADS, and boresight FSM loop tracking mirror position to estimate LED inertial motion
- Performance with high frequency FSM and LAFSM loops closed
- on-orbit closed loop performance estimated by taking the lab performance estimate against an inertial source and applying weighting function representing the time lag between the transmit and receive pulse times

(This page intentionally blank)

Time and Frequency Domain Analysis (con't)

Time Domain studies demonstrate

- Open loop receiver jitter for an inertial source (excluding non-common optics) is the sum of the open loop boresight signal and the LED inertial motion
- Consistency between the receiver open loop jitter estimates from the frequency domain and the receiver open loop time histories

Time simulation closes the three main body loops against a flexible representation of the payload and satellite

- Main body open loop crossovers set at 0.02 Hz
- Bending filters taken from the AXAF-I Powered Flight Model provide ample gain and phase margins on all three axes
- Scan and derotator loops closed in structural model using 2.5 Hz and 2.9 Hz stiffness, respectively. The damping for these modes set at 0.707

Satellite Main Body Controller
On-Board Computer (OBC) Implementation

The OBC implementation of the main body controller is shown in the block diagram. The digital interface between the reaction wheel drive electronics and the structural model is represented by the synchronized samples (a zero-order-hold, not shown, follows each sampler). The reaction wheel electronics is shown symbolically. Also, the bending filters, not shown, operate on the state x_{c2}. The gyro frequency limitation is not included so that bounding performance could be estimated.

The main body controller is a PII controller. The proportional loop operates on the rate error. The integral path represents the weighted position error, and the double integral path represents the weighted integral position error.

Satellite Main Body Controller
On-Board Computer(OBC) Implementation

The integrated output from a PII controller provides momentum commands to the reaction wheel OBC loops

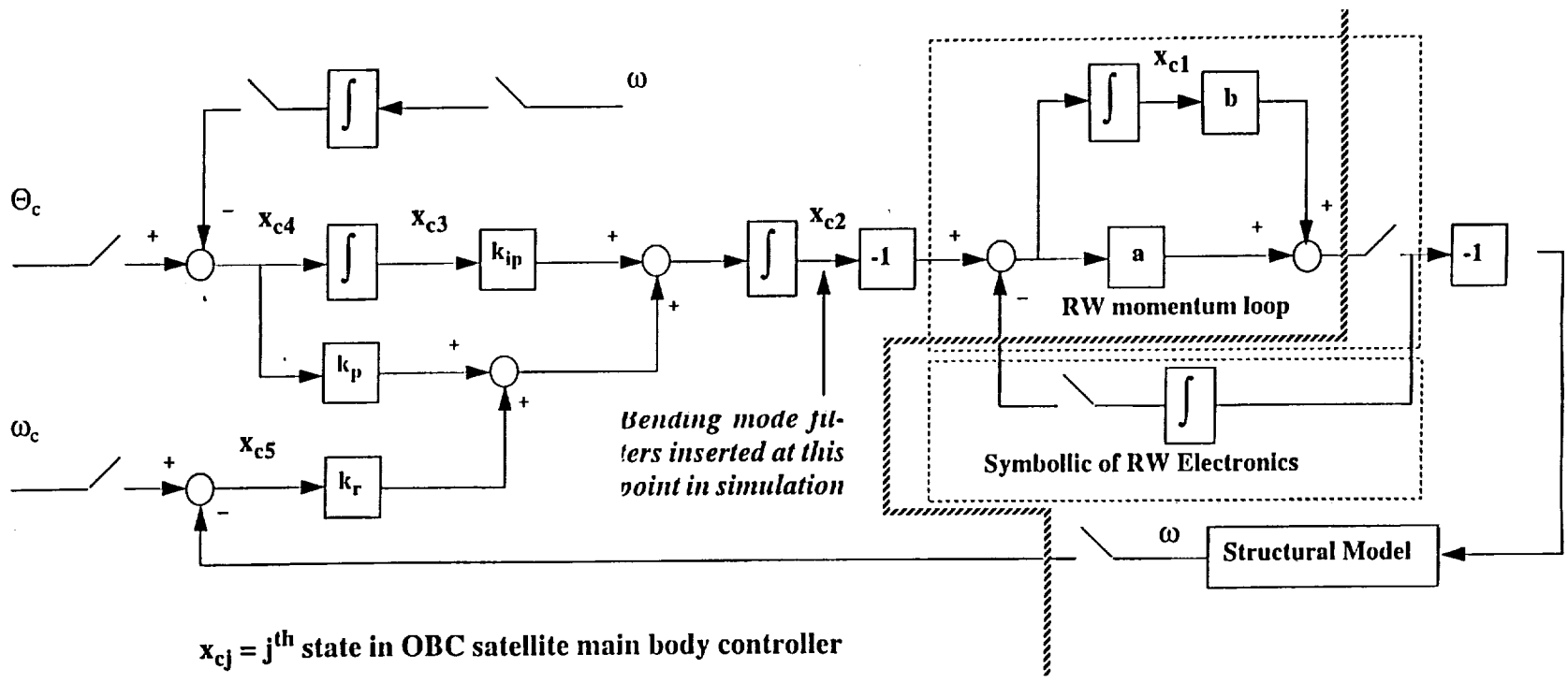

Performance Against Inertial Source in Lab

There are two distinct aspects of the receiver jitter problem. The first estimates performance in a laboratory setting where the receiver jitter is measured for a fixed inertial source. On-ground verification of loop performance with actual hardware can be accomplished at minimal cost using an inertial source. The far-field, open loop receiver signal, computed in the time simulation, are shown in the vugraph. For our simplified model, the sum of the LED inertial motion and the boresight sensor signal reproduces the two receiver signals shown. Modeling of the derotator optics in the receive path through the BAPTA, which was not included in this study, will produce a slight difference is signature between the LED inertial plus boresight LOS and the receiver-sensed LOS motions.

The open loop receiver signal in X is $\approx$ 12 μrad and, in Y_p, is approximately 36 μrad.

Performance Against Inertial Source in Lab

Open loop boresight signal minus LED inertial motion matches receiver signals

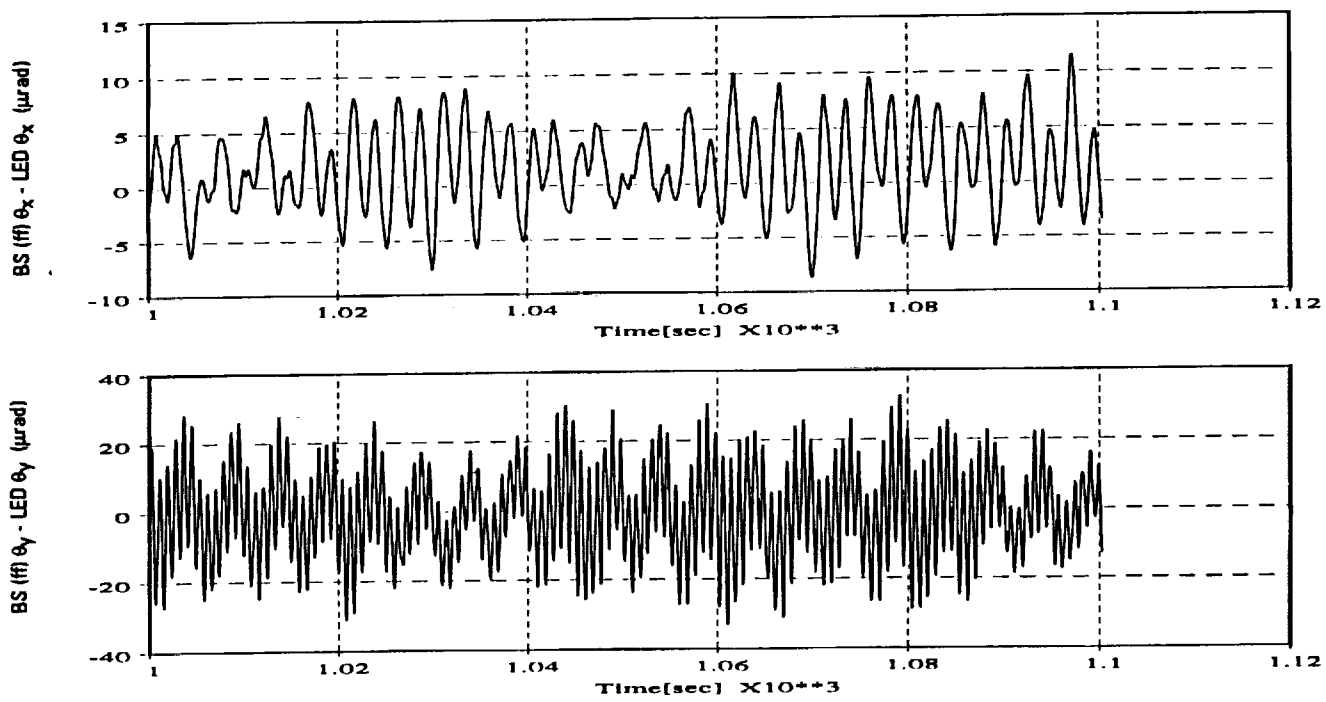

On-Orbit Performance

The on-orbit open-loop receiver performance estimate is shown on the vugraph. It is computed by taking the receiver LOS at time, t, and subtracting the transmitter LOS delayed 5 msec. All the key disturbances are acting on the satellite except the non-repeatable bearing disturbance.

The estimated on-orbit open loop receiver jitter is approximately 120 nrad in X and $\approx$ 1 μrad in Y_p. The downlink antenna, mounted on a boom out along the X-axis, contributes to the motion about Y_p.

On-Orbit Performance

Receiver open loop performance estimated as receiver LOS at time (t) minus transmitter line of sight at time (t-0.005) seconds. Reaction wheel, SADAs and the BAPTA harmonics (n = 1,2,3) modeled. Telescope primary mirror support structure mode at ≈ 13 Hz not excited for this example

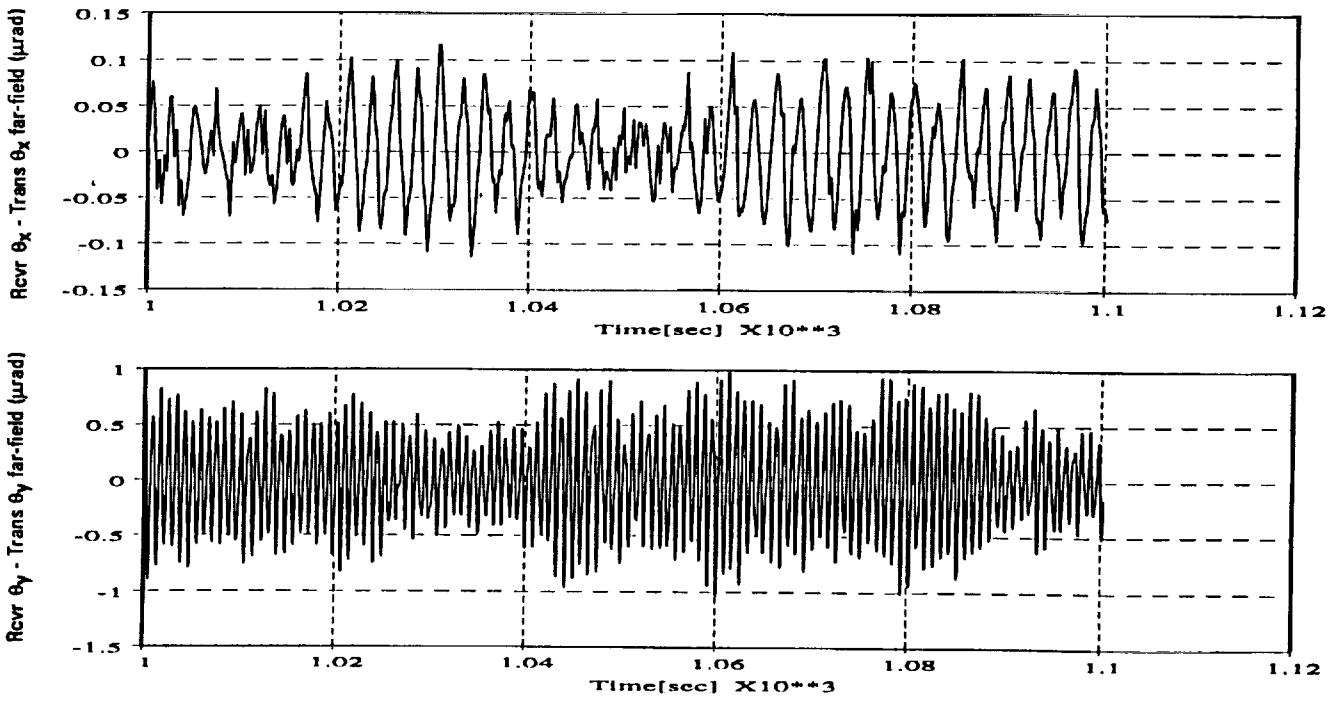

IRU and LED Inertial Motions

The next two vugraphs compare the X (satellite roll) axis and the Y_p-axis LED inertial motion with the inertial motion about the same axes at the IRU structural node.

The LED motion is the sum of 1) the inertial motion at the IRU, 2) the relative motion between the IRU and the optical bench, and 3) the relative motion from the optical bench to he LED. With the FSM closed about the boresight sensor, the alignment from the optical bench to the LED is measured by the FSM position readout sensor--the bicapacitive sensor.

IRU and LED Inertial Motions

Structural path between IRU on main satellite bus and LED mounted on metering structure near the primary mirror causes difference in inertial motions

X-axis response

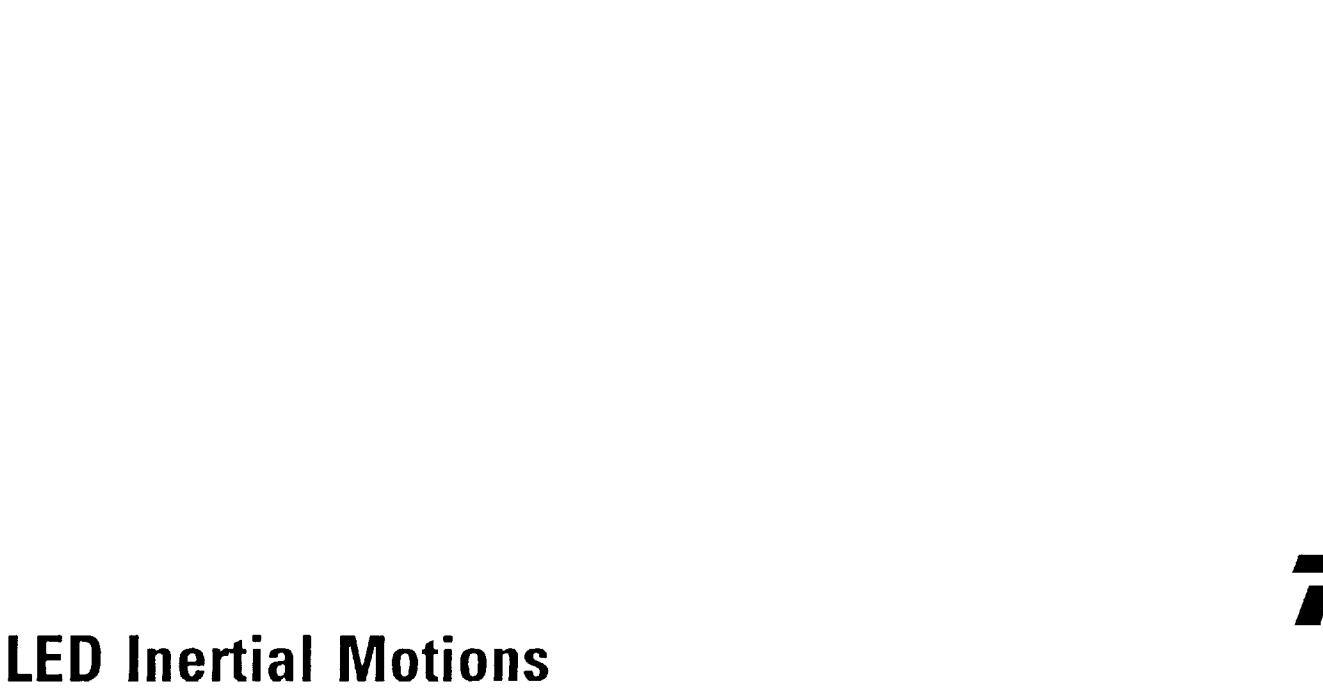

C-2

IRU and LED Inertial Motions (con't)

The frequency content of the motion at the IRU node projected on the Y_p axis is noticeably different from the LED motion about Y_p. Since the LED is relatively near the ADS, the LED motion over the ADS bandpass can be combined with the optical bench to LED alignment data from the FSM bicapacitive sensor and the IRU data on the satellite bus to estimate the LED motion from dc through the ADS bandpass. Blending filter constants, discussed in the following Steady State Controls Analysis Section can be calibrated by measuring performance against an inertial source.

IRU and LED Inertial Motions (con't)

Y-axis response

ADS provides LED motion above 3 Hz but IRU fails to provide good estimate of LED motion from dc through gyro bandwidth of 15 Hz

- Fast Steering Mirror steady state analysis addresses LED motion estimation using (ADS + IRU) signals and measured FSM position data

(This page intentionally blank)

TRW

Fast Steering Mirrors
Steady State Controls Analysis

(This page intentionally blank)

(This page intentionally blank)

Single Axis Control Loop Model

The overall fast steering mirror control loops for a single axis are shown here. The top and bottom paths at the final summing node comprise the "open loop" disturbances consisting of the structural motion and the motion of the boresight alignment LED, respectively. The path coming in from the left represents the control action which attempts to null the disturbances.

The design objectives are:

- Compensate structural vibration to 500 Hz using the LED and boresight sensor with the fast steering mirror (FSM) in the image motion compensator loop to less than 0.5 μrad (rms-far field)

- Compensate inertial motion down to DC using blended inertial reference unit (IRU), angular displacement sensor (ADS) and FSM bicapacitive sensor data. Command lag angle fast steering mirror (LAFSM) to center return beam on receiver. Maintain stability and attenuate disturbance to less than 0.5 μrad (rms-far field) within the controller bandwidth

As will be shown, the design objectives are attained with a margin of a factor of approximately 1.5 or a short-term jitter of approximately 0.3 μrad (rms-far field) when the largest expected disturbance sources--the BAPTA or scan bearing noise, the solar array stepping and the spacecraft reaction wheel unbalance and torques--are considered.

Cross coupling of torques applied to the FSM and LAFSM are shown in the diagram. However, these reaction torques are expected to be several orders of magnitude less that those of the above disturbances and, therefore, were neglected in this study.

Single Axis Control Loop Model

$\tilde{\theta}_{BS}$ = BS signal with FSM at zero position

TRW Fast Steering Mirror Frequency Response

The frequency response of a fast steering mirror used in several TRW programs is shown here. The mirror weight, for this application, is estimated to be approximately 4.5 lbs. Note the structural harmonics which appear around 1500 Hz. These limit the performance bandwidth of the mirror. Fast steering mirrors exist which can achieve wider bandwidths, however, the bandwidth of the mirror shown here is adequate for this application.

TRW Fast Steering Mirror Frequency Response

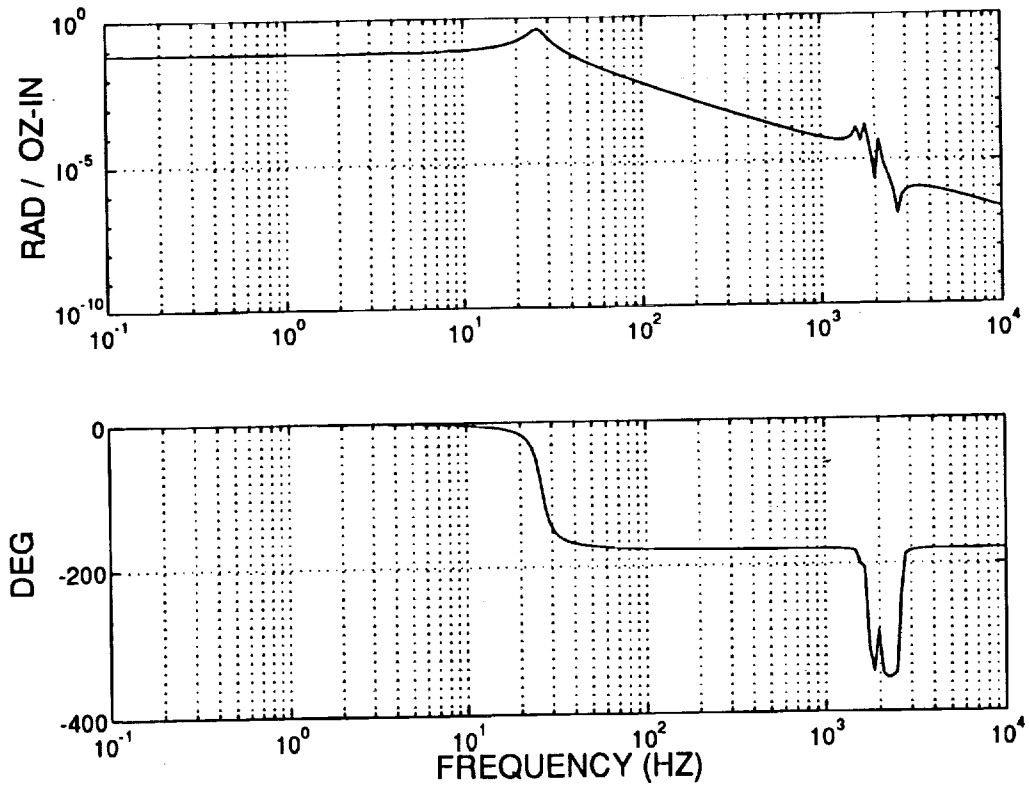

Lag Angle Fast Steering Mirror (LAFSM) Compensation

The LAFSM loop compensation is a straightforward loop design problem. The gain needs to roll off before the structural modes which occur at 1500 Hz. Integral control is used to ensure high open loop gain so that tracking is good at low frequencies.

The loop parameters are:

$I = 5.30 \times 10^{-4}$ in-lb-sec^2/rad

$D = 15.1 \times 10^{-3}$ in-lb-sec/rad

$K = 14.2$ in-lb/rad

Lag Angle Fast Steering Mirror (LAFSM) Compensation

- LAFSM COMPENSATION

- DESIGN GOAL: MAKE $\frac{e_2}{u_2}$ AS SMALL AS POSSIBLE OVER A 100 HZ BAND

  USE INTEGRAL (TYPE I) CONTROL FOR HIGH OPEN LOOP GAIN

LAFSM Controller Performance

The LAFSM controller performance is shown on the facing vugraph. The performance parameters are, considering the mirror assembly as a rigid body:

Controller order = 3

Gain margin = 7.3 dB

Phase margin = 55°

The first significant parasitic modes are expected to occur at approximately 1500 Hz.

LAFSM Controller Performance

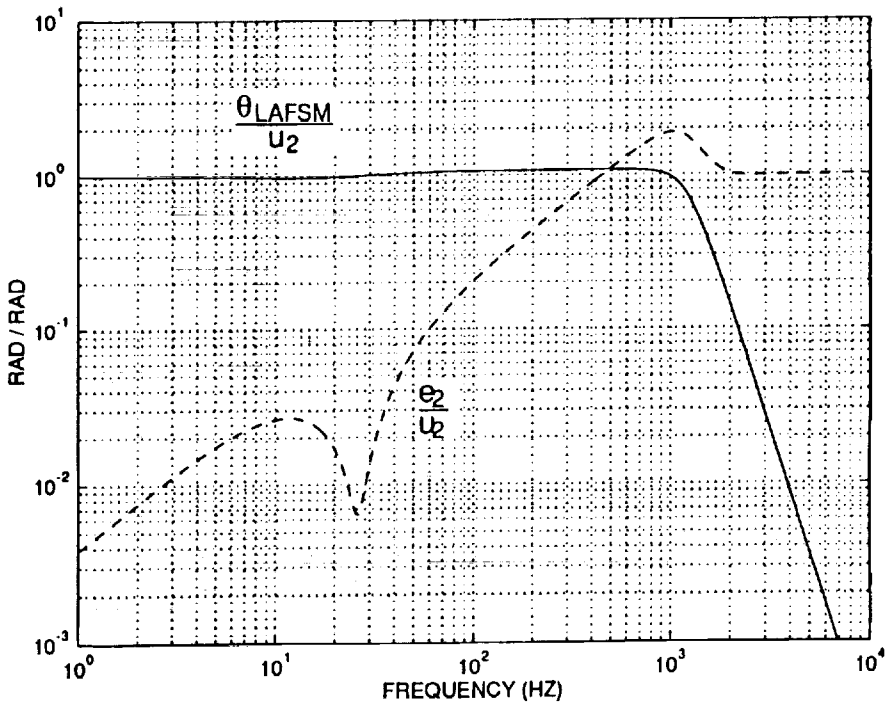

Fast Steering Mirror (FSM) Compensation

In the FSM loop compensation design, the loop is closed around the boresight sensor which is assumed to have a 2nd order butterworth response with a corner frequency of 500 Hz.

The loop parameters are:

$I = 5.30 \times 10^{-4}$ in-lb-sec^2/rad

$D = 15.1 \times 10^{-3}$ in-lb-sec/rad

$K = 14.2$ in-lb/rad

Fast Steering Mirror (FSM) Compensation

- FSM COMPENSATION

NOTE: OPTICAL SENSITIVITIES IGNORED FOR PURPOSES OF DESIGN

- DESIGN GOALS: MAKE $\frac{\tilde{\theta}_{FSM}}{\theta_{FSM}}$ AS SMALL AS POSSIBLE OVER BORESIGHT SENSOR BANDWIDTH

  ROLL OFF LOOP GAIN BEFORE 1000 HZ TO MAINTAIN STABILITY FROM MIRROR & STRUCTURAL MODES

FSM Controller Performance

The FSM loop controller performance is shown on the facing vugraph. The performance parameters are, considering the mirror assembly as a rigid body:

Controller order = 5

Gain margin = 4.1 dB

Phase margin = 50°

As with the LAFSM, the first significant parasitic modes are expected to occur at approximately 1500 Hz. The FSM is closed about the boresight sensor in contrast to the LAFSM which is closed about the bicapacitive sensors.

FSM Controller Performance

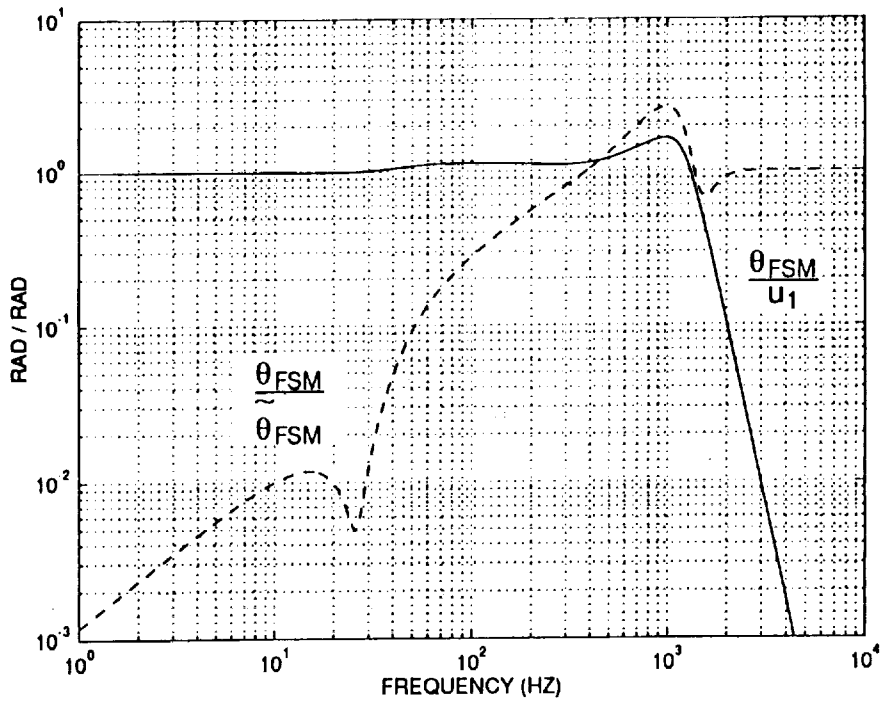

Receiver Short-term Jitter Error Spectrum

This function represents the greatest relative excursion of a sinusoid at the given frequency within the 5.2 msec round trip time of the laser pulse. The dashed line in the graph is an envelope function given by

$$E(s) = \frac{2s}{s + \frac{2\pi}{3\Delta t}}$$

which may easily be put in matrix differential form to ease computations of the effective rms errors.

Receiver Short-Term Jitter Error Spectrum

Evaluation of performance

- Evaluate receiver short-term jitter error spectrum from all disturbances

Additional consideration

- The maximum movement of the primary mirror under a sinusoidal vibration of the form $\Delta\theta = A\sin(\omega t)$, in the pulse round-trip time interval $\Delta t = 5.2$ msec is

This function may be applied to produce an equivalent reduction of the disturbances at the receiver

Angular Displacement Sensor (ADS) & Inertial Reference Unit (IRU) Frequency Responses

The ADS is assumed to have corner frequencies of 3 Hz and 2000 Hz, and the IRU model is assumed to have a corner frequency of 15 Hz. These are assumed characteristics but are typical of these sensors. The design is not particularly dependent the sensor characteristics, except insofar as they can be modeled accurately.

Angular Displacement Sensor (ADS) & Inertial Reference Unit (IRU) Frequency Responses

The ADS and IRU are assumed to have the frequency responses shown below

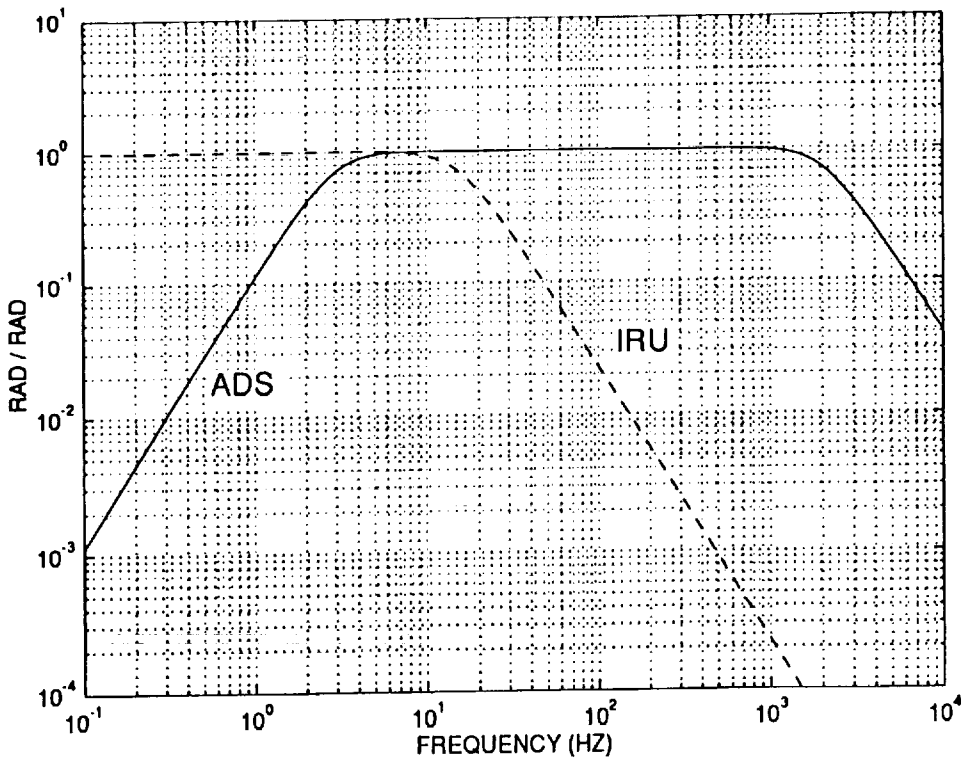

BAPTA Scan Drive Torque Disturbance Spectrum

The scan drive disturbance was assumed to have a flat frequency content distributed between 1.2 and 12 Hz with an rms value of 1.4 μrad and harmonics at multiples of the scan frequency of 0.2 Hz falling off at the index of the harmonics cubed, with an aggregate rms value of 14.5 μrad. These rms values are converted to in-lbs by the stiffness of the BAPTA.

The scan drive disturbance is the most significant jitter error source considered. The PSD shown here is believed to be conservative--the actual bearing disturbances should not exceed the magnitude or the bandwidths shown here.

Slight damping was added to the harmonics to ease the computations of the effective rms disturbances.

BAPTA Scan Drive Torque Disturbance Spectrum

Solar Array Drive Assembly (SADA) Drive Torque Disturbance Spectrum

For this disturbance, the solar array drive is assumed to be stepped at 0.015 degree increments to achieve 360° during the orbital period leading to a sawtooth error disturbance with the fundamental harmonic at 4.2 Hz

Seven harmonics are modeled as significant. Slight damping was added to the harmonics to ease computations of the effective rms disturbances.

Solar Array Drive Assembly (SADA) Drive Torque Disturbance Spectrum

Reaction Wheel Torque Disturbance Spectrum

The spectrum of the reaction wheel torque disturbances was assumed to be distributed as shown on the facing vugraph.

Reaction Wheel Torque Disturbance Spectrum

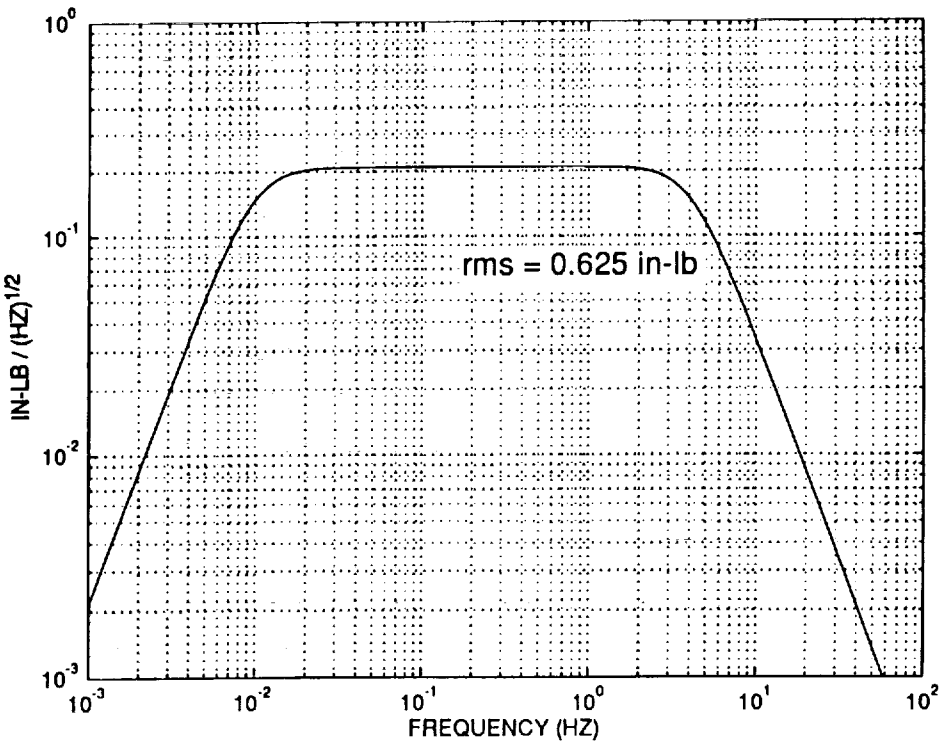

Structural Responses Due to Scan Bearing Disturbances

The X-axis structural response at various structural nodes resulting from the X-axis scan bearing disturbance are shown here. The finite element dynamics model includes modes only up to 100 Hz, as evident in the response curves. This, however, is where most of the strain energy is concentrated.

Note that the disturbance at the IRU node is much less observable than the disturbances at the other sensor nodes. This means that, at low frequencies, the IRU is relatively insensitive to LED motions in inertial space. It is necessary to blend boresight sensor data derived from the bicapacitive sensors of the FSM mirror when the loop is closed with the inertial data.

Structural Responses Due to Scan Bearing Disturbances

X-axis structural responses at selected nodes due to scan bearing disturbances about the x-axis

RECEIVER NODE

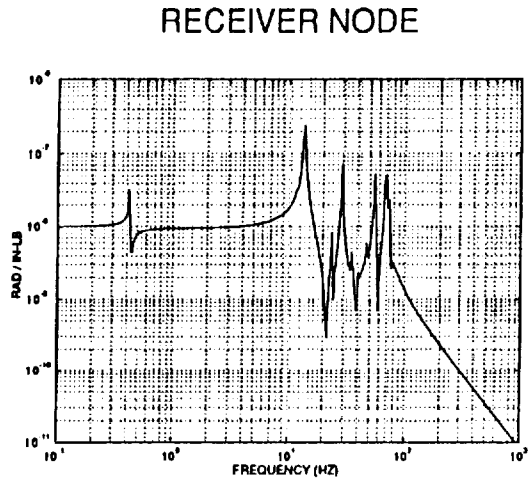

BORESIGHT SENSOR NODE

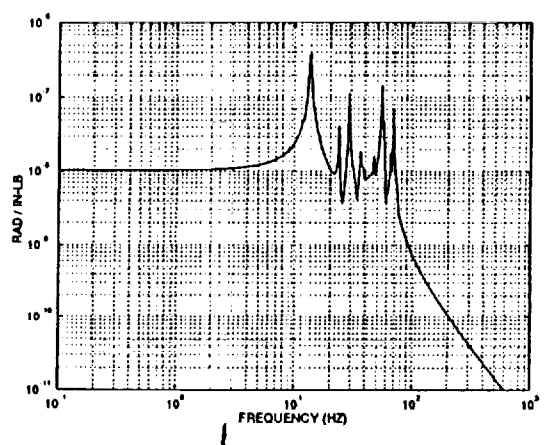

LED NODE

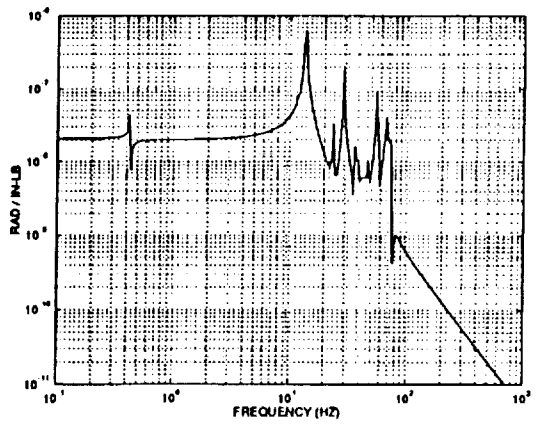

IRU NODE

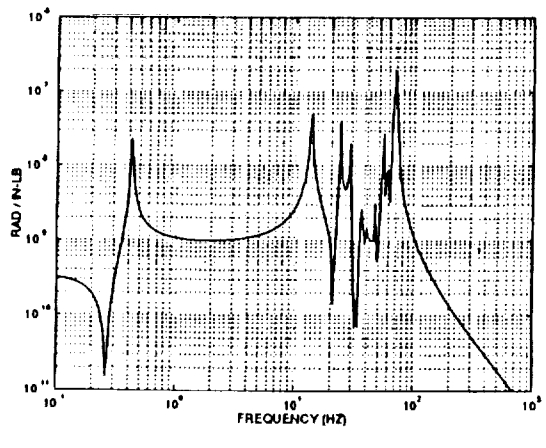

Blending Filter Block Diagram

Inertial sensor data from the spacecraft IRU and the ADS at the boresight sensor source (LED) must be blended with the relative motion data between the LED and the boresight sensor for the FSM loop closure. The blending filter architecture used is shown below.

The boresight sensor/LED ensemble corrects for the relative motion of the structure. In order to correct for the inertial motion, we need to estimate what the LED displacements are. The ADS provides information down to 3 Hz. The IRU provides low frequency information *at the IRU location.* The FSM mirror position provides the link between the ADS and IRU.

The filter gain may be selected by a variety of methods. An H_∞ design technique was initially investigated since it does not constrain the input noise spectrum. The H_∞ is best used when significant components of the input noise are localized in frequencies separated from the dominant plant response band.

In this case, however, the dominant error contributor is a plant structural mode at 13 Hz excited by the flat spectral region of the scan bearing disturbance. Consequently, an H_2 (Kalman) filter design proved to yield the best performance.

Blending Filter Block Diagram

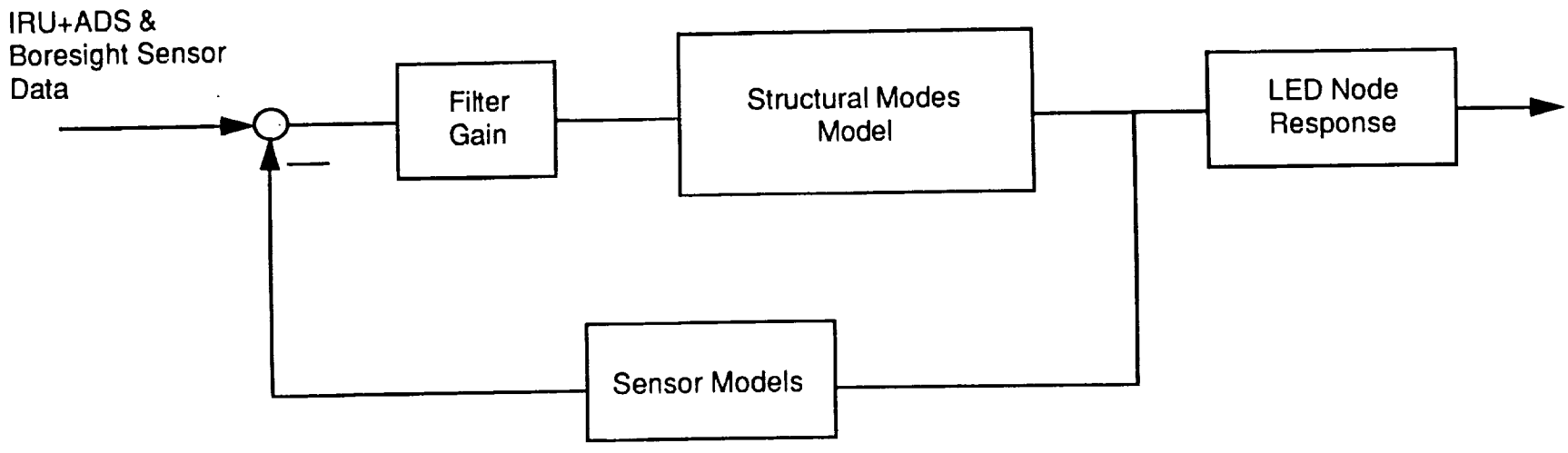

Estimator Design Considerations

The IRU and ADS sensors both provide information that can be unobservable at any of the other sensors. Therefore, the approach used to obtain the estimator was to use these measurements directly, and then to use only the boresight sensor information and the combined IRU plus ADS data to estimate the *residual* LED motion.

A comparison of the frequency responses for the X-axis scan bearing disturbance for these three sensors and the LED motion to be estimated is shown on this vugraph. A reduced order structural model in which all modes except the dominant 13 Hz payload mode was suppressed was used for the estimator optimization. All the disturbances and the key structural modes were included in the jitter performance analysis.

Estimator Design Considerations

Disturbance responses used for estimator design and X-axis blending filter optimization

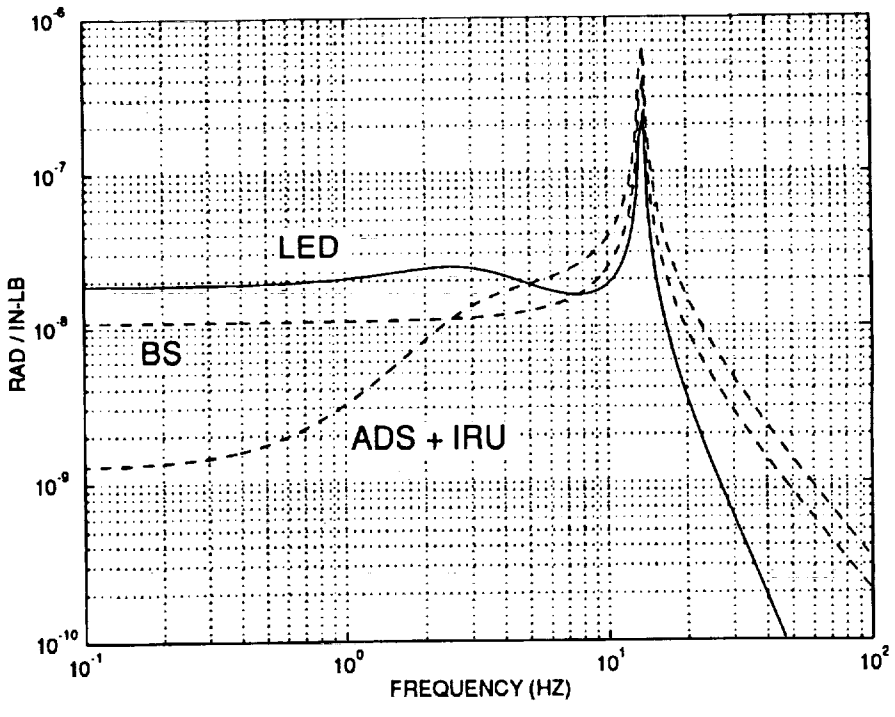

X-Axis Blending Filter Responses

The two blending filter responses, F_1 for the IRU-ADS sum and F_2 for the boresight sensor, are shown below. The filter, F_1, blends the IRU and ADS data to produce a smoothly varying response across all frequencies and the filter, F_2, acts upon the boresight sensor data to produce an estimate of the structural motion between these two nodes. As desired, the responses fall off above approximately 20 Hz.

All sensor measurements are combined into the same filter design algorithm because any single measurement has non-minimum phase characteristics (right-half plane zeroes) due to the structural model that would limit the performance of any single measurement estimator.

For the filter design, the FSM loop and LAFSM loop were treated as unity gains. As indicated in the control loop diagram at the beginning of this section, the actual quantities used in the filter are then effectively the IRU-ADS sum and boresight sensor data.

The filter design is quite robust. There are no peaks in the responses to create sensitivity.

X-Axis Blending Filter Responses

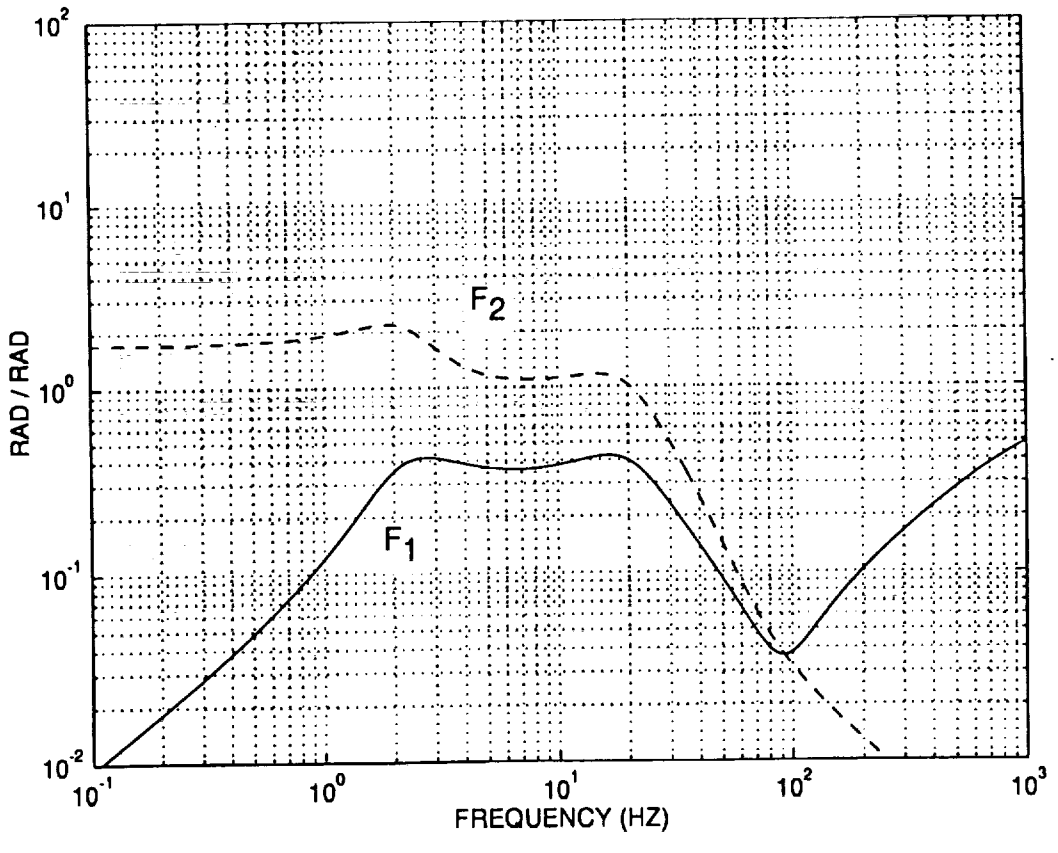

Single Axis Open & Closed Loop Jitter Spectrum (X-Axis)

The X-axis far-field jitter spectrum is shown below with the fast steering mirror loop both open and closed. The open loop jitter is shown by the dashed curve, and the closed loop response is shown by the solid curve. The disturbances about all three of the spacecraft axes (as appropriate) from the scan bearing, the reaction wheels and the solar array stepping are included.

As indicated on the figure, the open loop rms jitter is 2.4 μrad and the residual short-term rms jitter when the FSM loop is closed is ≈0.2 μrad.

Open and closed loop X-axis jitter contributions from the three disturbance sources, individually, are shown on subsequent vugraphs.

Single Axis Open & Closed Loop Jitter Spectrum (X-Axis)

Scan Bearing Induced Jitter Contributions

The dominant X-axis jitter source for the entire system is seen to be the 13 Hz disturbance excited by the scan bearing broad band disturbance about the x-axis. This disturbance is the most significant contributor to the overall jitter. As before, the open loop response is shown by the dashed curves and the closed loop residual jitter is shown by the solid curves. The closed loop residual rms jitter is reduced by approximately an order of magnitude below the open loop response.

Scan Bearing Induced Jitter Contributions

Open and closed loop X-axis jitter responses due to scan bearing disturbances about the X and Y-axes

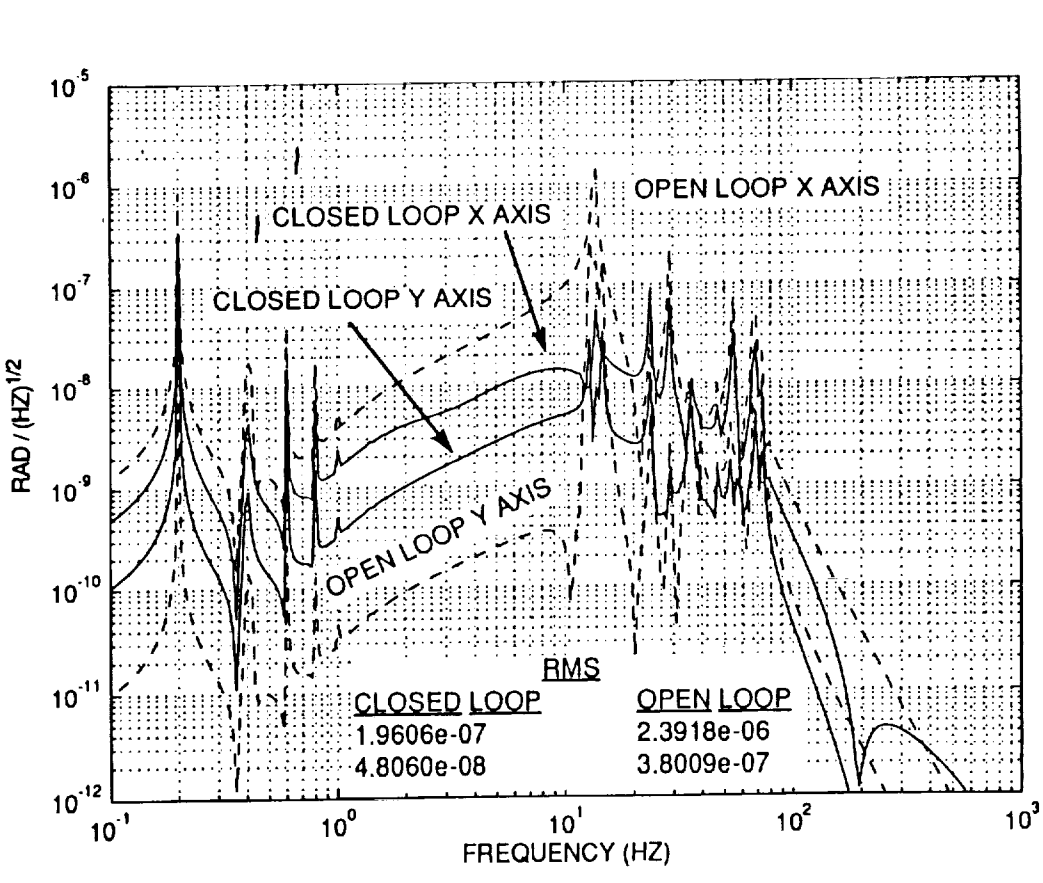

SADA Induced Jitter Contributions

The open (dashed curve) and closed (solid curve) loop X-axis jitter resulting from solar array-induced disturbances at both the +Y and -Y locations are shown here. On the diagram, the closed loop jitter appears to be worse than the open loop response. At the dominant mode near 13 Hz, the closed loop performance is improved over the open loop, and this is where the major jitter contribution is concentrated. The integrated closed-loop performance is improved over the open-loop performance by approximately a factor of two as indicated by the rms values of about 9 nrad open loop to about 4 nrad closed loop.

SADA Induced Jitter Contributions

Open and closed loop X-axis jitter responses due to SADA-induced disturbances at the +Y and -Y locations

Reaction Wheel Induced Jitter Contributions

As with the previous two vugraphs, the open and closed loop X-axis jitter contributions are shown for disturbances about the X, Y, and Z spacecraft axes. The rms jitter contributions from the reaction wheels are seen to be small compared to the scan bearing disturbances.

Reaction Wheel Induced Jitter Contributions

Open and closed loop X-axis jitter responses due to reaction wheel disturbances about the X, Y, and Z axes

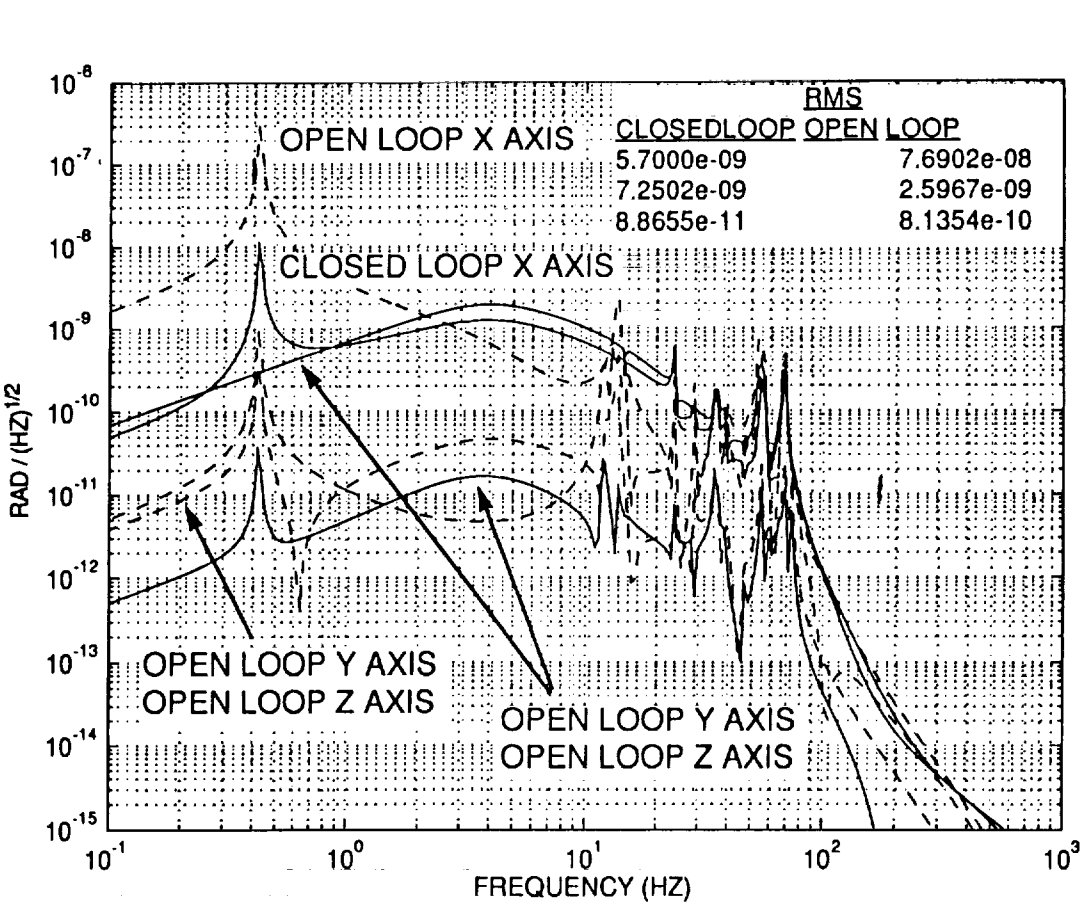

Single Axis Open & Closed Loop Jitter Spectrum (Y-Axis)

The Y-axis far-field jitter spectrum is shown below with the fast steering mirror loop both open and closed. As on the previous vugraph, the open loop jitter is shown by the dashed curve, and the closed loop response is shown by the solid curve. The disturbances about all three of the spacecraft axes (as appropriate) from the scan bearing, the reaction wheels and the solar array stepping are again included.

The Y-axis jitter, both open and closed loop, is less than the short-term jitter about the X-axis. As indicated on the figure, the open loop rms jitter is ≈ 0.5 μrad and the residual short-term rms jitter when the FSM loop is closed is ≈ 0.2 μrad.

The RSS value of the residual rms short-term jitter, then, is ≈ 0.3 μrad, meeting the specified jitter requirement for the 2 μm LAWS system.

Single Axis Open & Closed Loop Jitter Spectrum (Y-Axis)

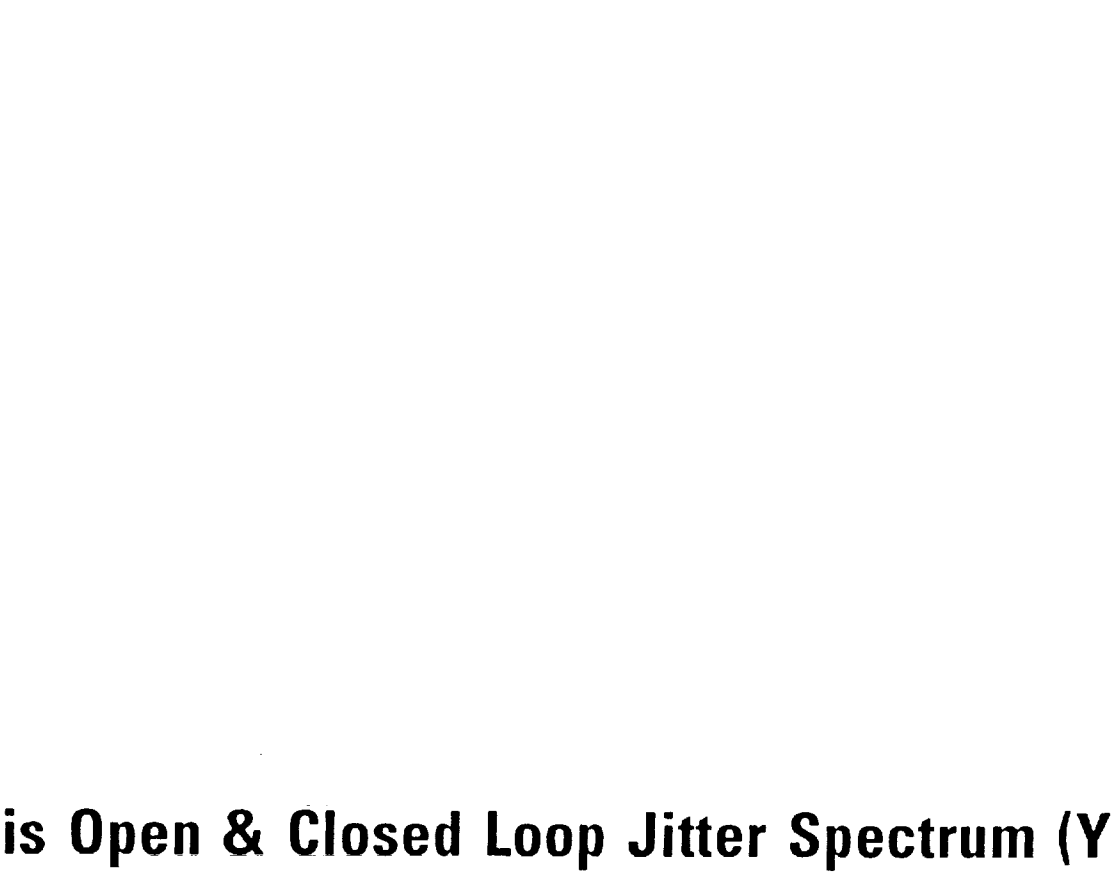

(This page intentionally blank)

Summary and Conclusions

(This page intentionally blank)

(This page intentionally blank)

Summary & Conclusions

A conceptual, but detailed, structural model of the 2 μm LAWS instrument assembly, which conforms to the design parameters derived in the 2 μm LAWS System Study (6 October 1993), was developed and used to construct a finite element dynamics model. This was merged with an existing dynamics model for a TRW UAB-940 spacecraft and used to investigate the short-term jitter performance of the solid state LAWS payload/spacecraft system in a realistic spacecraft environment.

Disturbance sources included in the analysis were the bearing and power train assembly (BAPTA) or scan bearing noise, spacecraft reaction wheels unbalance and torques, and solar array stepping torques. The scan bearing noise was found to dominate the other disturbances.

A fast steering mirror control loop system was designed to provide for the short-term jitter control and its performance analyzed subjected to the above disturbance environment. The performance analysis shows that the short-term jitter over the 5.2 msec pulse round-trip time can be controlled to within approximately 0.3 μrad rms. This is within the short-term jitter requirement of ≤ 0.5 μrad rms defined in the 2μm LAWS System Study required to yield a S/N loss < 0.3 dB.

Summary & Conclusions

Conceptual structural/dynamics model for 2 μm solid state LAWS payload defined and implemented

- Merged with existing TRW UAB-940 spacecraft bus dynamics model
- LAWS payload/AB-940 bus compatible with Delta-class launch vehicle

Disturbance models defined for

- BAPTA (scan bearing) noise
- Spacecraft reaction wheel torques
- Solar array drive torques

- Scan bearing disturbance greatest contributing jitter source

Fast steering mirror control loops designed to compensate for short-term jitter

Controls analysis shows that for realistic spacecraft environment

- Short-term jitter performance over 5.2 msec pulse round-trip time $\approx$ 0.3 μrad rms
- Within specified value of $\leq$ 0.5 μrad rms to yield S/N loss < 0.3 dB

REPORT DOCUMENTATION PAGE

Form Approved
OMB No. 0704-0188

1. AGENCY USE ONLY *(Leave blank)*	2. REPORT DATE	3. REPORT TYPE AND DATES COVERED
	January 1995	Contractor Report

4. TITLE AND SUBTITLE
Two-Micron Laser Atmospheric Wind Sounder (LAWS) Pointing/Tracking Study

5. FUNDING NUMBERS
C NAS1-19291

WU 233-01-01-03

6. AUTHOR(S)
Scott Manlief

7. PERFORMING ORGANIZATION NAME(S) AND ADDRESS(ES)
TRW Space & Technology Division
Space & Electronics Group
One Space Park
Redondo Beach, CA 90278

8. PERFORMING ORGANIZATION REPORT NUMBER

9. SPONSORING / MONITORING AGENCY NAME(S) AND ADDRESS(ES)
National Aeronautics and Space Administration
Langley Research Center
Hampton, VA 23681-0001

10. SPONSORING / MONITORING AGENCY REPORT NUMBER
NASA CR-195012

11. SUPPLEMENTARY NOTES
Langley Technical Monitor: William L. Grantham

12a. DISTRIBUTION / AVAILABILITY STATEMENT
Unclassified - Unlimited

Subject Category 18

12b. DISTRIBUTION CODE

13. ABSTRACT *(Maximum 200 words)*

The objective of the study was to identify and model major sources of short-term pointing jitter for a free-flying, full performance 2μm LAWS system and evaluate the impact of the short-term jitter on wind-measurement performance. A fast steering mirror controls system was designed for the short-term jitter compensation. The performance analysis showed that the short-term jitter performance of the controls system over the 5.2 msec round-trip time for a realistic spacecraft environment was = 0.3 μrad, rms, within the specified value of <0.5 μrad, rms, derived in a 2μm LAWS System Study (6 October 1993). Disturbance models were defined for 1) the Bearing and Power Transfer Assembly (BAPTA) scan bearing, 2) the spacecraft reaction wheel torques, and 3) the solar array drive torques. The scan bearing disturbance was found to be the greatest contributing noise source to the jitter performance. Disturbances from the fast steering mirror reaction torques and a boom-mounted cross-link antenna clocking were also considered but were judged to be small compared to the three principal disturbance sources above and were not included in the final controls analysis.

14. SUBJECT TERMS
Pointing Jitter, Atmospheric Remote Sensing, Laser Wind Sounder

15. NUMBER OF PAGES
168

16. PRICE CODE
AO8

17. SECURITY CLASSIFICATION OF REPORT	18. SECURITY CLASSIFICATION OF THIS PAGE	19. SECURITY CLASSIFICATION OF ABSTRACT	20. LIMITATION OF ABSTRACT
Unclassified	Unclassified		